Project 059(B) Jet Noise Modeling and Measurements to Support Reduced LTO Noise of Supersonic Aircraft Technology Development

Georgia Institute of Technology/Gulfstream Aerospace Corporation

Project Lead Investigator

Krishan K. Ahuja
Regents Professor
School of Aerospace Engineering
Georgia Institute of Technology
270 Ferst Drive, NW Atlanta, GA 30342-0150
404-290-9873
Krish.Ahuja@ae.gatech.edu

University Participants

Georgia Institute of Technology (Georgia Tech)

- PI: Krishan K. Ahuja, Regents Professor
- FAA Award Number: 13-C-AJFE-GIT-060
- Period of Performance: October 1, 2021 to September 30, 2022
- Tasks:
  1. Consultation with the advisory panel
  2. Defining nozzle requirements and design tests
  3. Design and fabricate a baseline mixer nozzle
  4. Test setup and experimental data acquisition
  5. Data dissemination
  6. Design and build a mixer for year 3 investigation
  7. Proposal for a follow-on effort for year 3
  8. Reporting and data dissemination

Project Funding Level

This project received $250,000 from FAA and $250,000 of cost-sharing from Gulfstream for the reporting period. (This is the same as received for the Year 1 effort.)

Investigation Team

- Dr. Krishan Ahuja, PI, Georgia Tech
- Dr. Jimmy Tai (co-PI), Georgia Tech
- Dr. Aharon Karon, co-investigator and lead experimentalist, Georgia Tech Research Institute (GTRI)
- Dr. Robert Funk, experimentalist, GTRI
- Reagan C. Mayo, graduate research assistant, GTRI
- Jackson Larisch, graduate research assistant, GTRI
- David N. Ramsey, graduate research assistant for portion of the program; subsequently a National Science Foundation Fellow working on fundamental issues related to the current project, Georgia Tech

Project Overview

The overall goal of this project is to perform cost-effective supersonic transport (SST) jet noise research/technology experiments to enable low-, medium-, and high-fidelity jet noise prediction methods. The specific objective is to design the

experiments in collaboration with industry, NASA, the Department of Defense (DOD), FAA, and modelers funded by the FAA to help develop improved jet noise prediction methods with reduced uncertainty and to enable industry to design quieter supersonic jet engines with higher confidence regarding the noise that will be generated. In collaboration with Gulfstream Aerospace Corporation (GAC), Georgia Tech's industry partner on this project, a representative baseline nozzle design will be selected for experiments at Georgia Tech. The data acquired will consist of far-field noise, high-speed flow visualization, source location, and detailed mean and unsteady flow measurements.

The experimental data acquired by Georgia Tech will be provided to key stakeholders and other computational teams funded by FAA to validate their computational simulations to confirm that jet noise predictions using semi-empirical and computational modeling approaches can be reliably used for jet noise evaluation.

This project has eight tasks, as listed below. The task titles are self-descriptive and reflect the task objectives. A short objective statement, research approach, and summary of the accomplishments to date for each task is provided after each task description. However, to put context to the tasks of the current period (Year 2), a brief summary of the tasks conducted in year 1 is provided below and we will refer to this as Task 0. To avoid confusion in the numbering of tasks for year 1 and year 2, roman numerals are used to refer to the tasks of year 1.

Task 0 - Summary of Year 1 Tasks

Georgia Institute of Technology

Objective(s)

The objectives of Year 1 tasks are outlined as subtasks listed below:

i. Form an Advisory Panel

This task has been completed.

ii. Identify a Baseline Nozzle Requirements and Design Tests

This task has been completed.

iii. Design and Fabricate a Baseline Nozzle

This task has been completed. This baseline nozzle was also used in year 2.

iv. Test Setup and Experimental Data Acquisition

The experimental facility is completely set up for the program. All acoustic measurements in the GTRI static anechoic chamber have been completed. The particle image velocimetry (PIV) data acquisition for the unheated core jet has been completed. Flow visualization for the unheated core jet has been completed. Halfway through the program, we suffered a few setbacks with respect to problems with the beamforming array as well as heat insulation of the flow diagnostic facility. The facility in the anechoic chambers was, however, OK, which allowed us to continue acquiring the acoustic data. Both setups are expected to become operational during the tenure of the current program. As improvements to the PIV post-processing scheme and schlieren photography were acquired during the 2022 reporting period, details on these will be included in the description of new results below.

v. Data Dissemination

The final model design was shared with the modeling teams in November 2021. All acoustic data, both for the unheated and heated-core conditions, have been shared with the modelers. All of the unheated core flow PIV data have also been shared with the modelers, and the flow visualization has been made available to the modelers.

vi. Assess Readiness of Design Tools for a Simple Baseline Nozzle Configuration

Whereas Task 5 just provides the data to the modelers, the objective of this task is to interact with the modelers in terms of verifying their codes with the measurements made under this project at Georgia Tech. Partners GAC and Aerospace Systems Design Lab (ASDL) will also be comparing their low-fidelity codes with our data.

vii. Proposal for a Follow-on Effort for Years 2 and 3

Proposals for both Years 2 and 3 were submitted.

viii. Reporting and Data Dissemination
All Year 1 reports (annual and quarterly) were submitted. See above or status of the data dissemination.

Research Approach
The research approach for the Year 1 effort has been described in detail in various Year 1 reports and consisted of seven technical tasks and one reporting task as summarized above under tasks with numbers in roman numerals.

Milestones
Described in Year 1 reports and consisted of completing the tasks as summarized above under tasks with numbers in roman numerals.

Major Accomplishments
These are described in various Year 1 reports and consisted of accomplishing the objectives of the tasks listed above with numbers in roman numerals. These accomplishments included building a model scale confluent nozzle, setup which was mounted in GTRI's anechoic chamber and also in a flow diagnostics facility. Considerable amount of farfield acoustic data complemented by PIV data was acquired, which was provided to the modeling team working on Project 59 for validating computational codes being developed by them. Data was acquired for a number of operating conditions and three mixing lengths. Certain conditions produced discrete tones, which were later identified to be associated with a feedback phenomenon.

Publications
None.

Outreach Efforts
None.

Awards
None.

Student Involvement
One graduate student (David Nate Ramsey) and an undergraduate student (Reagan Mayo).

Plans for Next Period
Conducting Year 2 effort described below.

Task 1 - Consultation with the Advisory Panel
Georgia Institute of Technology

Objective
The objective of this task is to receive regular feedback from industry and NASA subject matter experts in supersonic jet noise.

Research Approach
At the beginning of the Year 2 effort, a meeting was held with the whole ASCENT 59 project team and the advisory panel to discuss the direction of the research effort for the year. The project 59B team continued to discuss the project progress and direction with the advisory panel throughout the effort. Most meetings were organized and conducted by Dr. Sandy Liu of FAA.

Milestones
None. The team of modelers and experimentalists under this project were to meet during the tenure of the project on dates organized by Dr. Sandy Liu and discuss the progress and plans. The team met at least four times during the year.

Major Accomplishments
Project 59B team shared the results of the Year 2 effort with the advisory panel as well as the modelers.

Publications
None.

Outreach Efforts
None.

Awards
None.

Student Involvement
One graduate student (David Nate Ramsey) and an undergraduate student (Reagan Mayo).

Plans for Next Period
Meet on a regular basis as arranged by FAA.

Task 2 - Defining Nozzle Requirements and Design Tests
Georgia Institute of Technology

Objective
The objective of this task is to define the nozzle requirements and design the experiments.

Research Approach
During the Year 1 effort, the baseline nozzle and tests were based on a paper engine design created by the Georgia Tech ASDL guided by the ASCENT 10 project on engine cycle selection for a GT Medium SST (55-passenger class). For simplicity, it was decided that the GT nozzle model tested under this project would not have a plug. For the purpose of calculating the area of the outer (secondary flow) duct, the annular areas of the paper engine were used to calculate the area of the secondary flow duct in the model nozzle facility. The GTRI model is a 0.045 scale of the paper engine. The mixing length/exhaust nozzle exit diameter (L_e/D_e) are 0.7, 1, 2, and 3. As will be described below, during the Year 2 effort, tabs were added to the primary nozzle to increase the mixing between primary and secondary streams. The goal was to create a mixer nozzle with a simple geometry, with the goal of providing the modeling teams with a mixer nozzle that is not as geometrically complicated as a lobed mixer.

To be consistent with the Year 1 work, the same condition matrix was used for Year 2. Figure 1 shows the conditions used on a per configuration basis, as well as for each core temperature (unheated or 500˚F). As with the Year 1 experiments, these tests have been designed with variations in nozzle design and/or operating parameters in order to explore the accuracy of semi-empirical and computational tools for predicting jet noise. To better test the ability of the tabs to increase the mixing between the primary and secondary stream, most of the focus was in the $L_e/D_e = 0.7$ configuration, although the effects of increasing the mixing length were also explored. Additionally, the configuration of the tabs was varied.

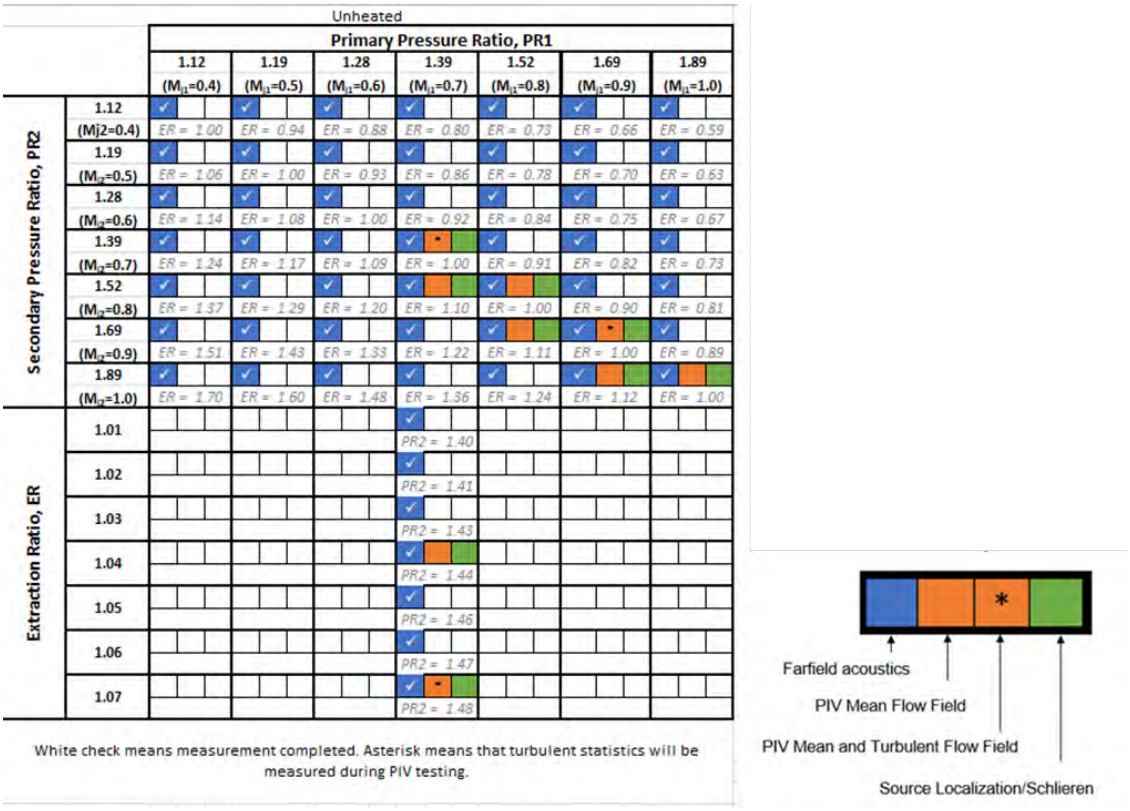

Figure 1. Test condition matrix. PIV, particle image velocimetry.

Milestones
Define the nozzle requirements and design the experiments at the start of the Year 2 effort.

Major Accomplishments
Completed defining nozzle requirements and design the experiments and selected the test matrix as outlined above.

Publications
None.

Outreach Efforts
None.

Awards
None.

Student Involvement
One graduate student (David Nate Ramsey) and an undergraduate student (Reagan Mayo).

Plans for Next Period
Plan for conducting tests with heated flow and with a Forced Mixer.

Task 3 - Design and Fabricate Baseline Mixer Nozzle

Georgia Institute of Technology

Objective

The objective of this task is to select the tab geometries that will added to the primary nozzle of the confluent nozzle.

Research Approach

For the purpose of creating a mechanical mixer nozzle with a simple geometry, tabs were added to the primary nozzle of the confluent nozzle. The baseline confluent nozzle that was used during the Year 1 effort is shown in Figure 2. The primary nozzle was transformed into a mixer nozzle by adding mechanical tabs to the nozzle exit. Two types of tabs were used for this purpose. The first are D-type tabs (referred to as "D-tabs"), which were tested by Ahuja and Brown (1989) who showed significant increases in jet mixing when installed at the exit of a single nozzle and are shown in Figure 3. The other type of tabs are delta-type tabs (referred to as "delta-tabs"), which are shown in Figure 4 and have been used in many studies (Hileman, 2003; Saiyed, 1999; Tam, 2000). Figure 5 shows where the tabs were positioned in the confluent nozzle.

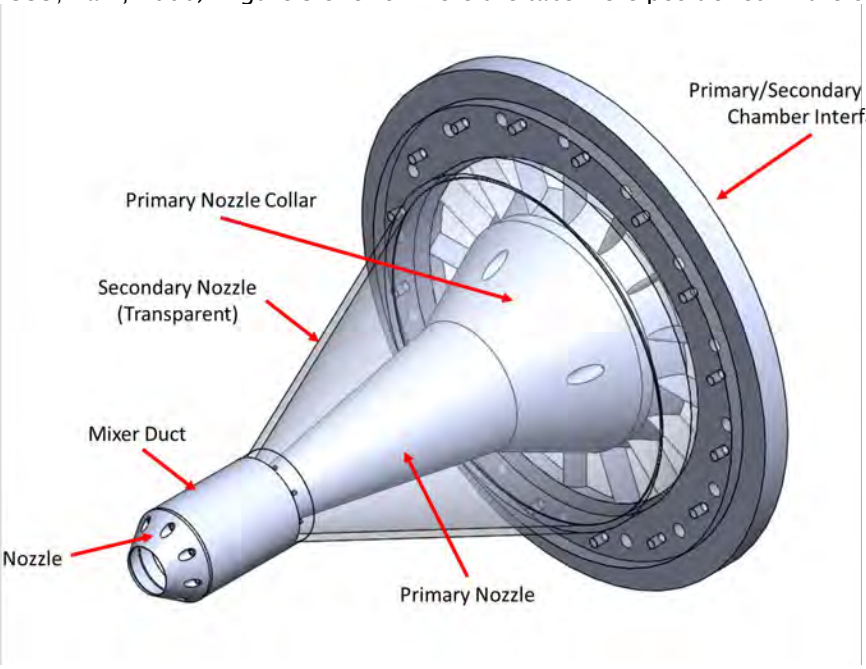

Figure 2. Experimental model design.

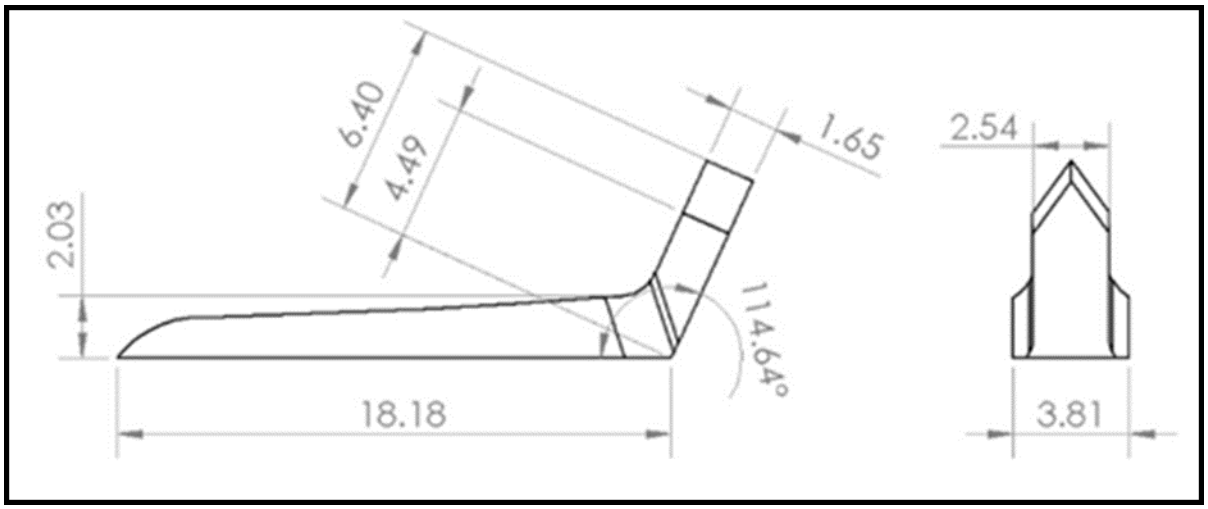

Figure 3. Design of the D-tab (dimensions in mm).

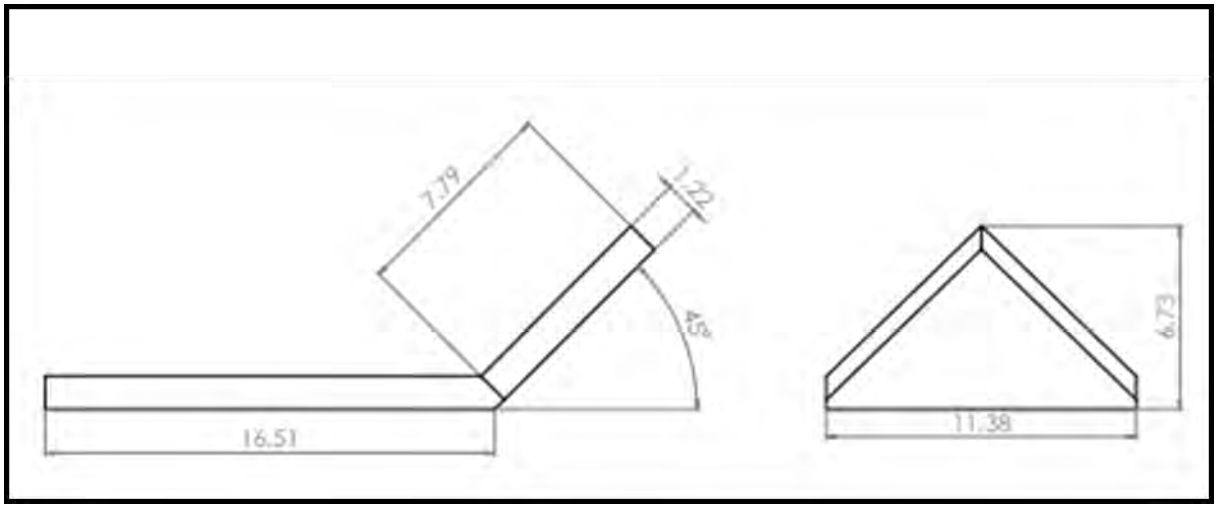

Figure 4. Design of the delta-tab (dimensions in mm).

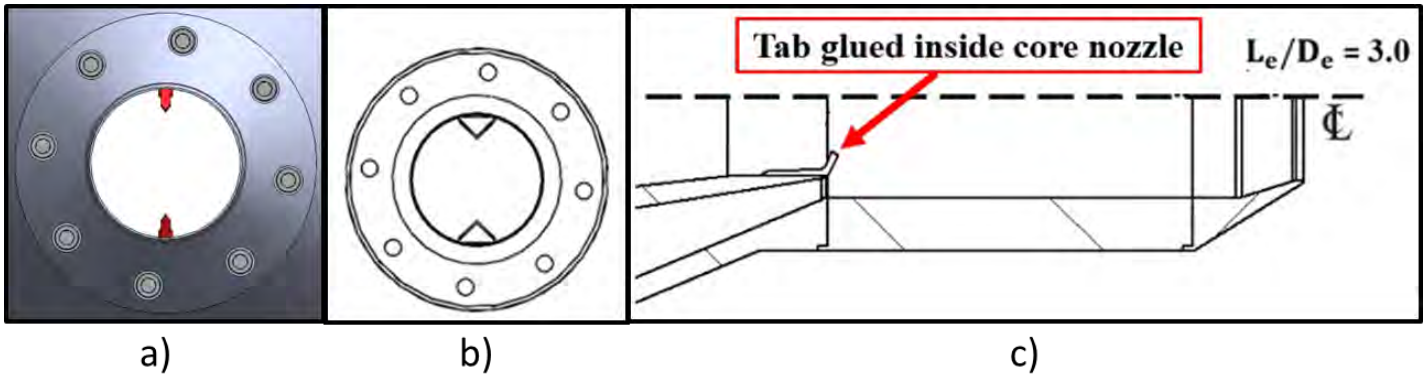

Figure 5. Tabs in the core nozzle: (a) D-tabs, (b) delta tabs, and (c) cross-sectional view of nozzle showing tab position.

Milestones
select and design a baseline mixer while waiting for our Cost-share partner Gulfstream to design and manufacture a forced multi-lobe mixer.

Major Accomplishments
Selected tabs as the baseline mixers as described above.

Publications
None.

Outreach Efforts
None.

Awards
None.

Student Involvement
Three graduate students (David Nate Ramsey, Reagan Mayo, and Jackson Larisch).

Plans for Next Period
None.

References
Ahuja, K., & Brown, W. (1989, March 13). Shear flow control by mechanical tabs. *2nd Shear Flow Conference*. 2nd Shear Flow Conference, Tempe, AZ, U.S.A. https://doi.org/10.2514/6.1989-994

Hileman, J., & Samimy, M. (2003). Effects of vortex generating tabs on noise sources in an ideally expanded Mach 1.3 jet. *International Journal of Aeroacoustics*, *2*(1), 35–63. https://doi.org/10.1260/147547203322436935

Saiyed, N., & Bridges, J. (1999, May 10). Tabs and mixers for reducing low bypass ratio jet noise. *5th AIAA/CEAS Aeroacoustics Conference and Exhibit*. 5th AIAA/CEAS Aeroacoustics Conference and Exhibit, Bellevue,WA,U.S.A. https://doi.org/10.2514/6.1999-1986

Tam, C. K. W., & Zaman, K. B. M. Q. (2000). Subsonic jet noise from nonaxisymmetric and tabbed nozzles. *AIAA Journal*, *38*(4), 592–599. https://doi.org/10.2514/2.1029

Task 4 - Test Setup and Experimental Data Acquisition

Georgia Institute of Technology

Objective

The objective of this task was to conduct the tests and acquire and analyze the data. So far, during the Year 2 effort, only acoustic measurements have been acquired. Because of a major failure in the GTRI Flow Diagnostic Facility (this was a failure that occurred after repairing another earlier failure), as reported in the quarterly progress reports, PIV data could not be obtained earlier. As noted above, extensive unheated core flow high-speed schlieren flow visualization was acquired as part of the Year 1 effort. Likewise, considerable improvements to the PIV data were made. As these two sets of data were acquired during this period of performance, these are reported in this report.

Research Approach

PIV Measurements

The PIV data were acquired in GTRI's Flow Diagnostics Facility using a double-pulsed, two-dimensional PIV system. The details of GTRI's Flow Diagnostics Facility were reported by Burrin et al. (1979) with salient details repeated here for completeness. The Flow Diagnostics Facility is a sister facility to GTRI's Anechoic Jet Facility, having identical plenum interfaces and identical plenum-to-nozzle area contraction ratios.

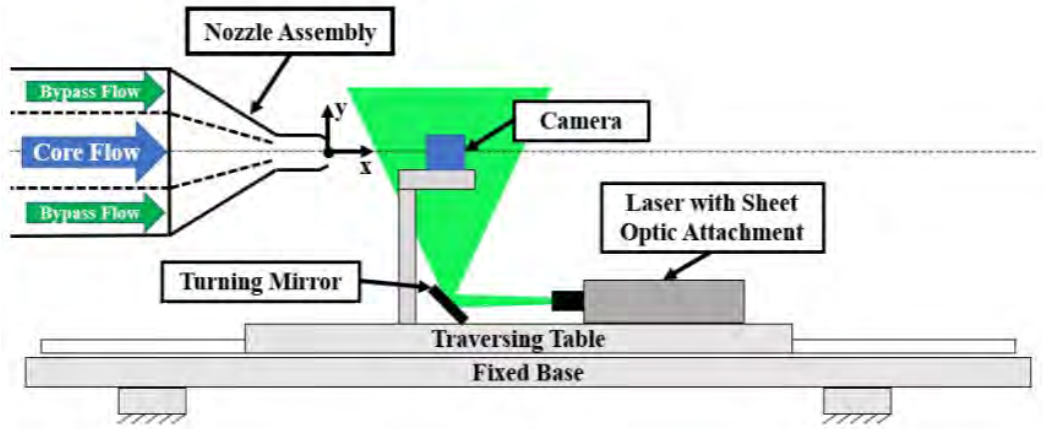

(a)

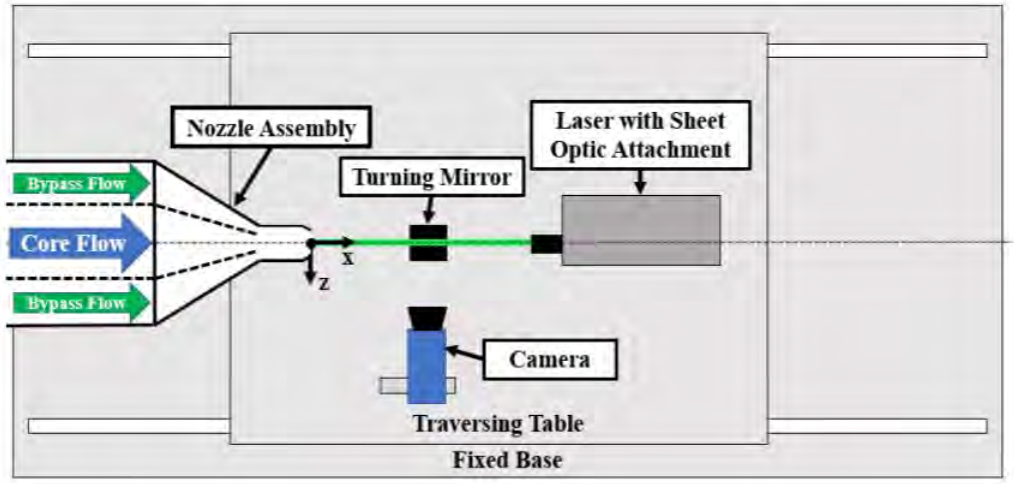

(b)

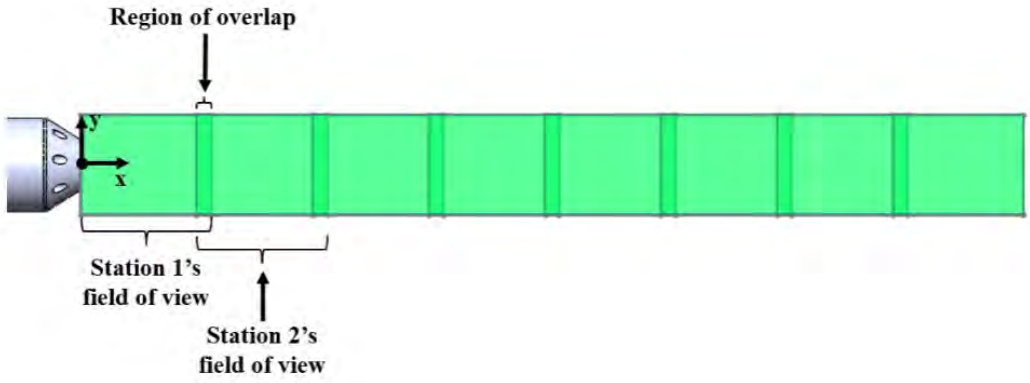

(c)

Figure 6. Particle image velocimetry (PIV) system: (a) side view, (b), top-down view, and (c) multi-station acquisition scheme.

The PIV system is shown schematically in Figure 6. Figure 6a and b show side- and top-down-view schematics of this system, respectively. Figure 6c illustrates the camera's nominal field-of-view at each of the stations along the traverse. In selecting the time delay between image pairs, an optimization routine built into the DaVis software was used. The DaVis software is the LaVision proprietary PIV software that is used for the data acquisition and post-processing. This routine recommends a time delay between image pairs based in part on the peak Q-ratio (the ratio of highest and second highest correlation peak values) for several different time delays. A low Q-ratio indicates that a particle displacement cannot be accurately predicted from the correlation plane of a given image pair in a given interrogation window.

The measured instantaneous velocity fields may contain spurious velocity vectors. Spurious vectors are characterized as having exceedingly large or small magnitude and/or erroneous direction relative to the expected velocity vector. Of course, the expected vector field is not known a priori, and criteria for identifying these spurious vectors must be employed. In this work, spurious vectors are detected and rejected at two different stages of the data processing routine. First, the instantaneous velocity fields are screened in a processing stage referred to as "vector post-processing." A filtering operation is used to detect and replace vectors that have a large deviation from their neighbors. This filtering operation is based on the framework of a dynamic mean value operator (Raffel, 2018). In particular, the filter was set to "strongly remove and iteratively replace" in the DaVis software – removing vectors that had a difference to the local mean outside of one standard deviation of the neighboring vectors before re-inserting vectors whose difference to the local mean is within two standard deviations of the neighboring vectors once the filter was applied. For vectors that failed to satisfy the criterion, the median of the neighbors was used to replace the vector. This filter was executed twice on each instantaneous velocity field. Further, a range of acceptable particle displacements was specified. Finally, any instantaneous vectors whose associated Q-ratio was less than 2.0 were deleted. The success of these vector post-processing operations in removing outliers without modifying the remainder of the velocity field is shown to be successful on a single, instantaneous velocity field in Figure 7. The top frame shows the result without the vector post-processing routine and the bottom frame shows the same field with the vector post-processing routine executed, both of which use the same color scaling shown on the far right. This vector field is a measurement across the shear layer of the jet from the core nozzle in isolation operated at $\boldsymbol{M_j}$ = 0.58, unheated, with the jet flowing from left to right in the figure. This portion of the data processing routine has remained unchanged since the first release of PIV measurements. However, refinements have been made that are outlined in the next paragraph.

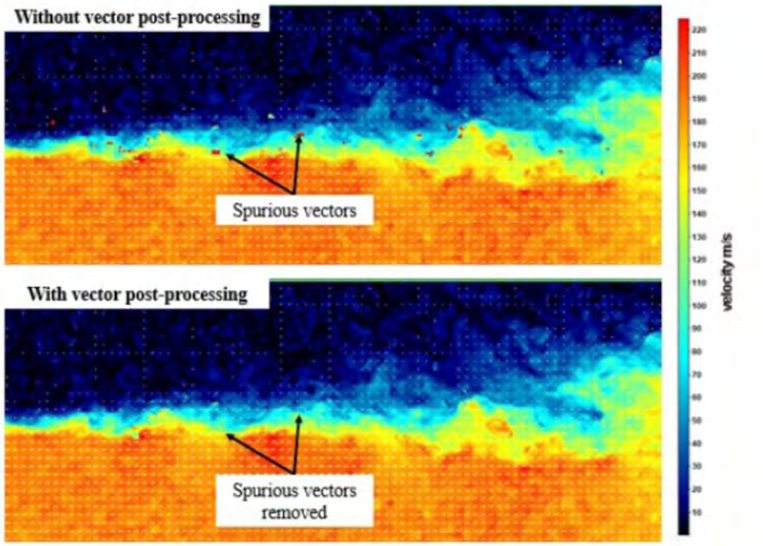

Figure 7. Success of vector post-processing in replacing spurious vectors. Both frames show the same region of shear layer of jet from single nozzle in isolation, M_j = 0.58, unheated.

The ensemble averaging of the PIV measurements now includes applying Chauvenet's criterion for spurious vector (i.e., outlier) rejection, which is believed to be an improvement over the more aggressive outlier rejection scheme used before this change. This change only has an appreciable impact on the measurements of velocity fluctuation (i.e., turbulence intensity), with relatively small changes to the mean velocity measurements. Chauvenet's criterion was reported to be used by Bridges and Wernet (2011) and is a sample size–dependent criterion that suggests thresholds outside of which values are unlikely to be sampled. If values are measured outside of these thresholds, the data are considered outliers. In each PIV interrogation window across all instantaneous velocity fields being ensemble averaged, Chauvenet's criterion is applied to each component of the measured velocity vectors. This criterion assumes that the measured velocities within each interrogation window are sampled from a Gaussian parent distribution. The reader astute in turbulent flows would likely dispute this assumption, and rightfully so. It is known that the turbulent velocities in a free shear layer are not always Gaussian distributed (as discussed in greater detail by Pope (2000)). In particular, the probability density function (PDF) of velocity at a point may have non-zero skewness, whereas a Gaussian distribution would have zero skewness. This potential criticism is acknowledged; however, a Gaussian PDF of velocities is not assumed aside from computing outlier rejection thresholds. Histograms of displacement in units of pixels, as acquired using the PIV measurement system, are presented in Figure 8. This figure shows that the use of Chauvenet's criterion correctly flags obviously spurious vectors (at the tips of the red arrows) without wrongly flagging seemingly trustworthy vectors (based on their presence in a larger distribution of data). Displaying the displacement histogram with units of pixels serves the secondary purpose of providing evidence that the PIV measurements are not affected by peak-locking effects. Were peak-locking present in the data, the displacement vectors would be biased toward integer displacement values (Raffel, 2018). Demonstrating this fact is vital to the integrity of the fluctuating velocity measurements produced, as Christensen (2004) showed that peak-locking may strongly affect second-order velocity statistics (i.e., the standard deviation of velocity reported in the present work).

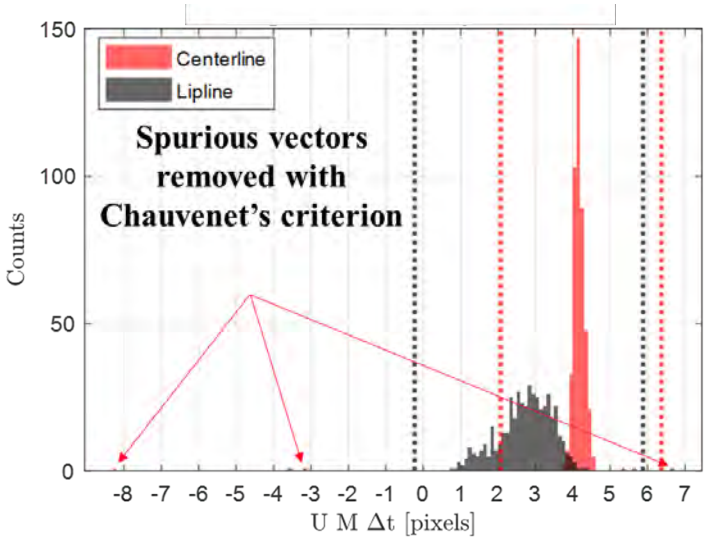

Figure 8. Histogram of axial displacement along lipline (x/D_e= 0.7, y/D_e=0.5, N=1500 image pairs) of jet from single nozzle (M_j = 0.58, unheated). Vertical lines show Chauvenet criterion boundaries.

Ahuja et al. (1982) acquired mean and unsteady velocity measurements of a jet produced by a convergent nozzle with an exit diameter of 2 inches (5.08 cm) in the GTRI Flow Diagnostics Facility using a laser Doppler velocimetry (LDV) system. As shown by Bridges and Wernet (2011), the LDV data of Ahuja et al. (1982) and several other sources of published jet flow-field measurements agree reasonably well when normalized. Thus, in the present work, agreement between flow-field measurements reported by Ahuja et al. (1982) and a validation dataset acquired using the present work's PIV system (when both are presented in normalized form) is taken to provide a high degree of confidence in the PIV measurements. This relies, of course, on the accuracy of historical datasets. The 1.6-inch nozzle used here is shown in Figure 9a and the agreement between the validation dataset is shown in Figure 9b. This agreement is even better than before Chauvenet's criterion was implemented in the data processing routine.

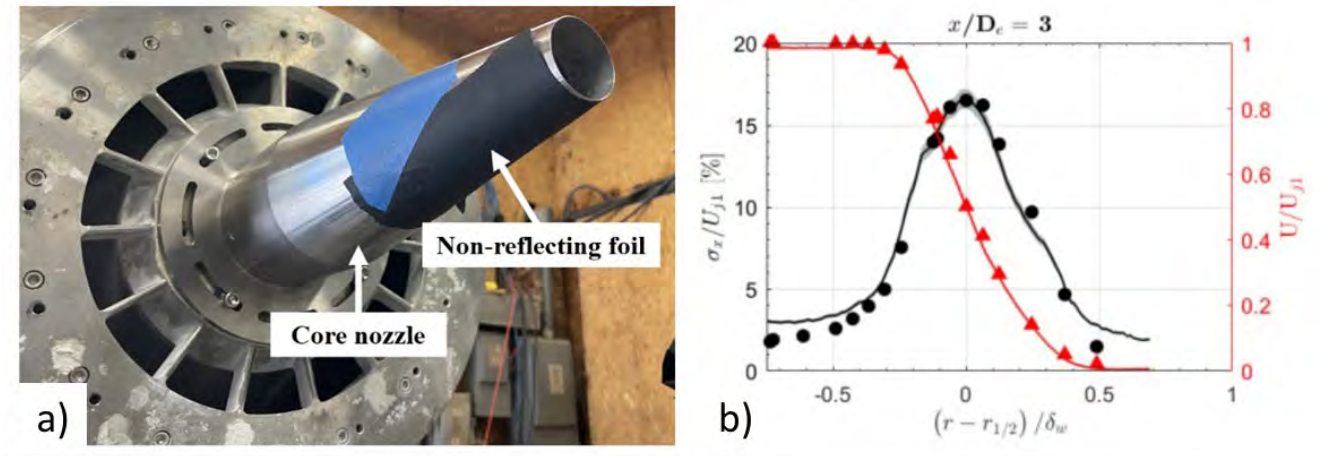

Figure 9. Validation dataset: (a) nozzle used, and (b) agreement with dataset from Ahuja et al. (1982). Curves are PIV data, and markers are historical LDV data from Ahuja et al. (1982). PIV, particle image velocimetry; LDV, laser Doppler velocimetry.

Figure 10 shows typical jet flow fields at a lower pressure ratio ($PR_1 = PR_2 = 1.39$, unheated), and Figure 11 shows what is believed to be a self-excited flow field at a high subcritical pressure ratio ($PR_1 = PR_2 = 1.69$, unheated).

Witze (1974) provided a model for the centerline velocity distribution of a compressible free jet, which was shown to agree well with experimental data. Bridges and Wernet (2011) used the potential core length obtained by the theory reported by Witze (1974) as a means to collapse PIV measurements acquired at different conditions. The "Witze model" (as it will be referred to hereafter) may be expressed as follows:

$$\bar{u}_c\left(\frac{x}{D_e}\right) = 1 - \exp\left(\frac{-1}{2\kappa\left(\frac{x}{D_e}\right)(\bar{\rho}_e)^{0.5} - X_c}\right) \tag{1}$$

$$\kappa = 0.08\left(1 - 0.16M_j\right)(\bar{\rho}_e)^{-0.22}$$

Here, $X_c = 0.70$, and the remaining parameters are defined in Witze's report. In the present work, claims about the shortening of the potential core of a jet under self-excited flow conditions are sought to be made. Using the measurements of the flow field alone, no direct evidence supporting such a claim can be found. There is no baseline, unexcited measurement that can be acquired for a self-excited condition – the excitation is always present. Were this an experiment involving a jet that was acoustically forced using a controlled sound source, measurements with and without the acoustic forcing could be acquired and compared. Instead, a different approach must be formulated using what is known about the behavior of the confluent nozzle. The self-excited condition to be characterized is the $PR_1 = PR_2 = 1.69$, unheated condition. It is known from other experiments that conditions with unity extraction ratio at lower pressures do not produce tones. Thus, if Witze's model for the centerline velocity distribution agrees well with the measurements at conditions with no tones, the model may be assumed to provide a reference for the shortening of the potential core of the jet caused by self-excitation.

The centerline mean velocity distribution of three different mixing lengths with unity extraction ratio at $PR_1 = 1.39$ are shown in Figure 12a and at $PR_1 = 1.69$ are shown in Figure 12b, along with Witze's model. It can be seen that all curves agree reasonably well with Witze's model for the lower pressure ratio, regardless of mixing length. However, the high subcritical condition shows a large departure from Witze's model, suggesting that a significant increase in mixing occurs at this condition relative to a single, unexcited jet. The farfield noise produced by the nozzle at this high subcritical pressure ratio is shown in Figure 13.

It is noted that there exists a mean axial velocity gradient close to the nozzle exit plane in Figure 12, and some explanations for this are offered. This phenomenon is believed to be a result of the contraction of the exhaust nozzle proximate to its exit plane. The contraction requires the fluid to turn radially inward near the upstream side of the exhaust nozzle and then to straighten out in a similar fashion near the exhaust nozzle exit plane. At these two locations, a force is required for the fluid to turn. Near the upstream side of the exhaust nozzle, the required force is supplied by the solid body of the nozzle. Near the exhaust nozzle exit plane, no solid body exists to supply the required force – it must instead come from the fluid itself in the form of a pressure gradient if the flow is to become approximately parallel as it exits the nozzle. The fluid near the center of the exhaust nozzle may supply the required pressure gradient if the fluid is at an elevated static pressure and thus has not yet reached its fully expanded velocity. Morris et al. (2010) measured a similar effect in the flow field produced by a single nozzle, and also attributed this effect to the nozzle's convergence at the nozzle exit plane.

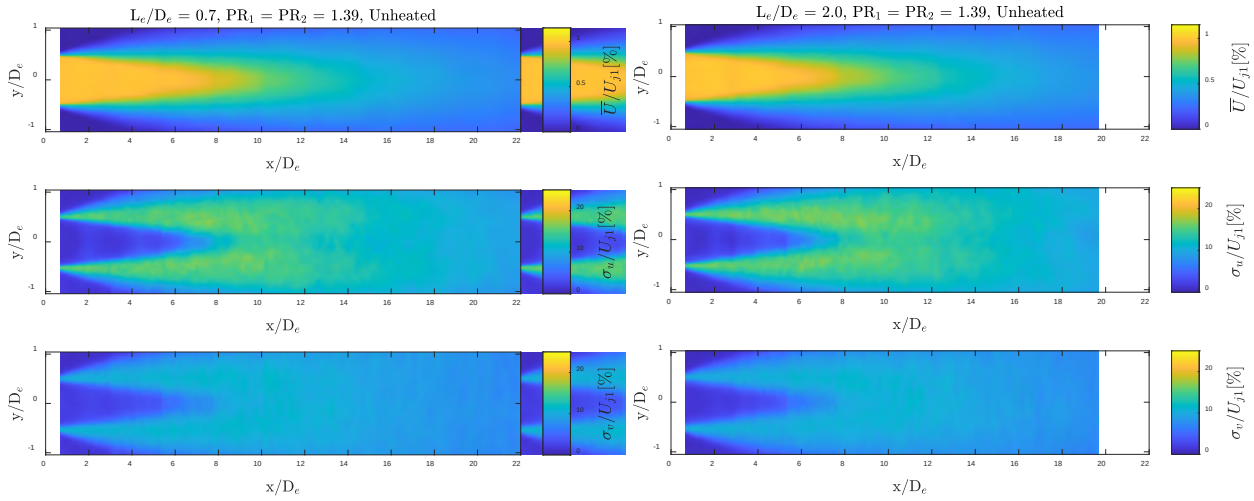

(a) **(b)**

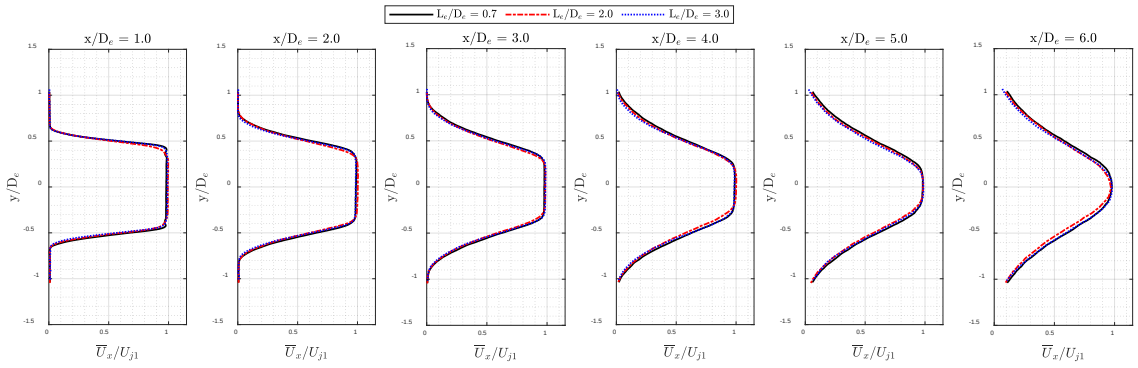

(c)

(d)

Figure 10. Typical flow field of jet from confluent nozzle ($PR_1 = PR_2 = 1.39$, unheated): (a) mean velocity, axial fluctuation intensity, and radial fluctuation intensity for $L_e/D_e = 0.7$; (b) mean velocity, axial fluctuation intensity, and radial fluctuation intensity for $L_e/D_e = 2.0$; (c) radial profiles of mean velocity near the nozzle exit for several mixing lengths; and (d) radial profiles of axial fluctuation intensity near the nozzle exit for three mixing lengths. N = 750 image pairs.

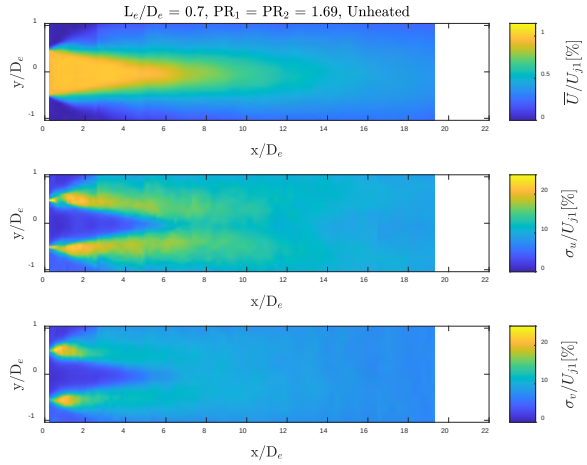

(a)

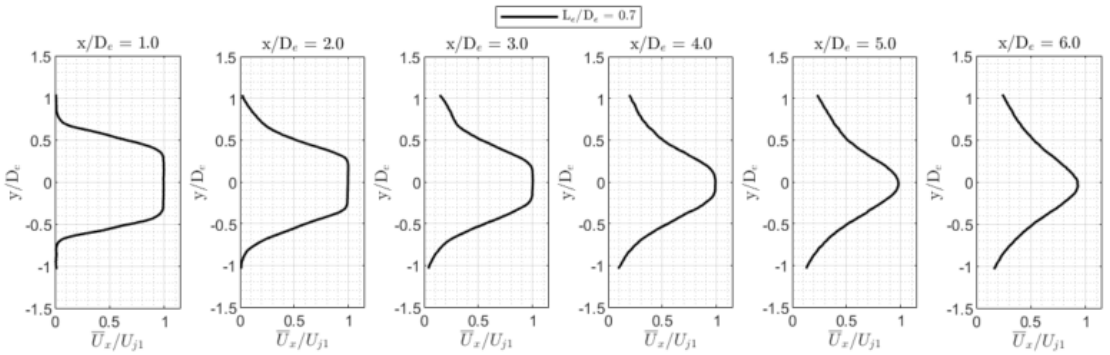

(b)

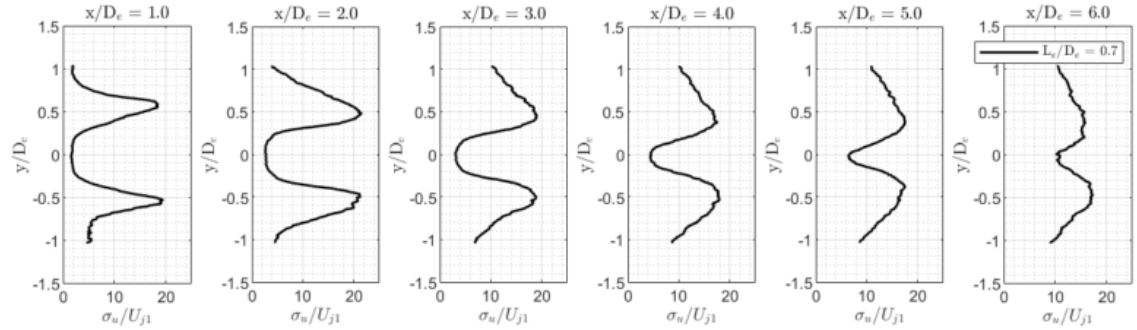

(c)

Figure 11. Self-excited flow field of jet from confluent nozzle ($PR_1 = PR_2 = 1.69$, unheated): (a) mean velocity, axial fluctuation intensity, and radial fluctuation intensity for $L_e/D_e = 0.7$; (b) radial profiles of mean velocity near nozzle exit; and (c) radial profiles of axial fluctuation intensity near nozzle exit. N = 750 image pairs.

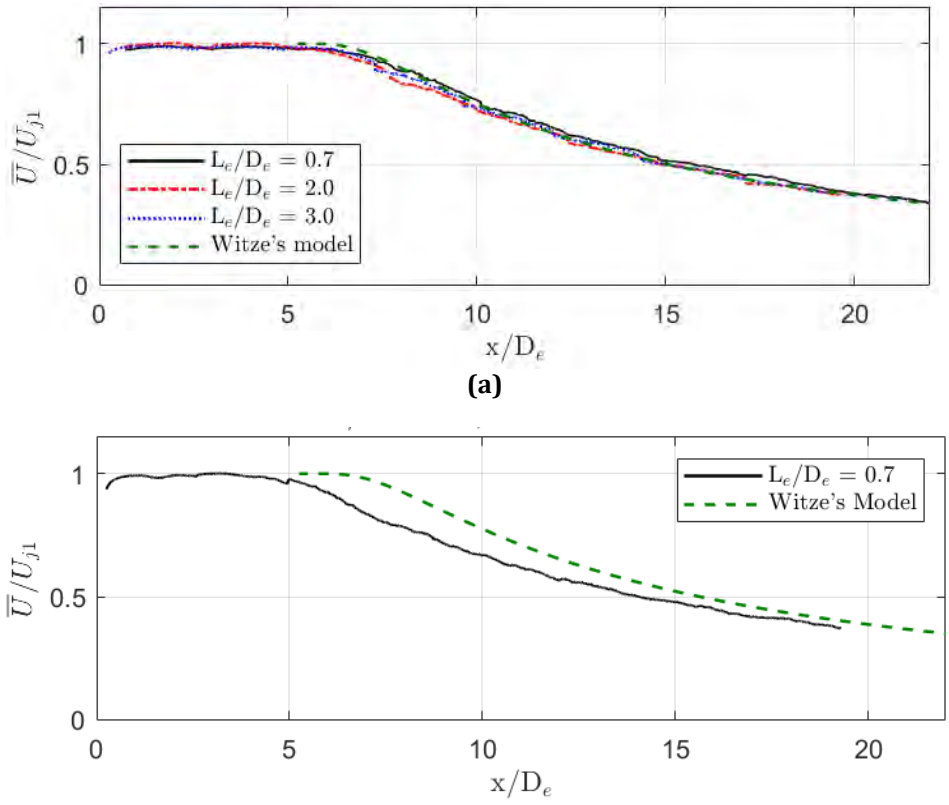

Figure 12. Centerline mean velocity distributions: (a) typical flow field including Witze's model for single jet ($PR_1 = PR_2 = 1.39$, unheated) and (b) self-excited conditions and Witze's model for single jet ($PR_1 = PR_2 = 1.69$, unheated). N = 750 image pairs.

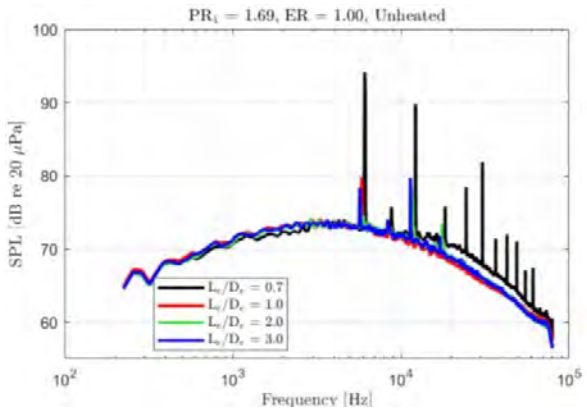

Figure 13. Lossless, fully corrected farfield jet noise spectra at high subcritical condition $PR_1 = PR_2 = 1.69$, unheated. $\theta = 90°$ (R = 84.7D_e).

High-Speed Schlieren Flow Visualization

GTRI's z-shaped schlieren setup is shown in Figure 14. An arc lamp light source emits light that follows a z-shaped path along a series of mirrors and lenses. The light source is positioned at the focal point of the first parabolic mirror, sending collimated light into the test section (the horizontal region between the two parabolic mirrors). The second parabolic mirror focuses the light rays (now refracted by density gradients within the test section) to a focal point. At the appropriate focal point, a knife-edge cutoff is positioned in one of two orientations: vertical (knife-edge normal to jet axis) or horizontal (knife-edge parallel to jet axis). These two knife-edge orientations reveal axial and transverse density gradients in the test section, respectively. The light is then passed through a pair of refocusing lenses that allow the camera to be placed far from the jet, which may be heated, in order to protect the camera. The schlieren images are captured on a Vision Research Phantom V2512 monochrome ultra-high-speed camera, with a resolution of 1,280 × 800 pixels at 25,000 frames per second and with a 1-μs exposure time. The video files being released to modeling teams will be in the .AVI format, with 100 frames total at 20 frames per second. While only short, 100-frame videos are being released, 2,500 images were recorded at each condition, and the longer duration measurements are available upon request. In the present work, only single snapshots from a few high-speed schlieren measurements are shown and discussed.

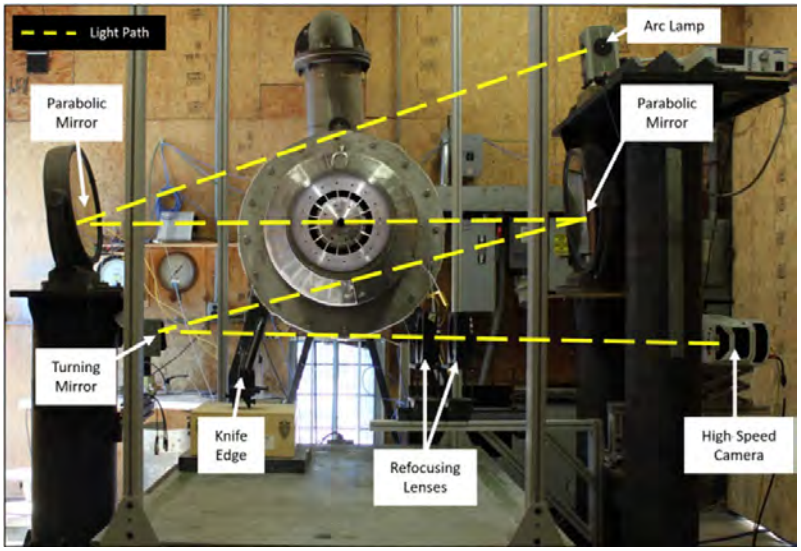

Figure 14. Georgia Tech Research Institute's z-shaped schlieren setup.

Representative schlieren snapshots are shown for the shortest mixing length (L_e/D_e = 0.7) and ER = 1.00 in Figures 15 to 17, each of which shows both transverse and axial density gradients. As the pressure ratio (and thus its Reynolds number) is increased, the turbulent density gradients become increasingly well defined. This is expected for two reasons. First, turbulent velocity fluctuations and their associated stresses on the fluid increase with Mach number. Second, the smallest scales of turbulence decrease with increasing Reynolds number ($Re = U_j D_e/\nu$). Relatively small changes are made to the apparent density gradients by increasing ER from 1.00 to 1.07 at the PR_1 = 1.39 condition, as shown in Figure 18. Similarly, little change is seen as ER is set to 1.10 (Figure 19). For the most part, the flow field at all of these conditions remains typical.

Figure 20 and Figure 21show examples of the self-excited conditions (PR_1 = 1.69, ER = 1.00) for two mixing lengths of L_e/D_e = 0.7 and 2.0, respectively. These conditions have larger jet spreading and apparent excited instability waves or coherent large-scale structures, which were absent in the flow for the other conditions. It is noted that increasing the pressures to a critical pressure ratio eliminates the tone and evidence of self-excitation (see Figure 17). It can be seen that the shortest mixing duct has greater jet spreading and stronger large-scale structures than the L_e/D_e = 2.0 mixing duct at the PR_1 = 1.69, ER = 1.00 condition.

Throughout these schlieren images, the axial density gradient near the nozzle exit plane is visible. An explanation for this effect is offered in the previous section on the PIV measurements.

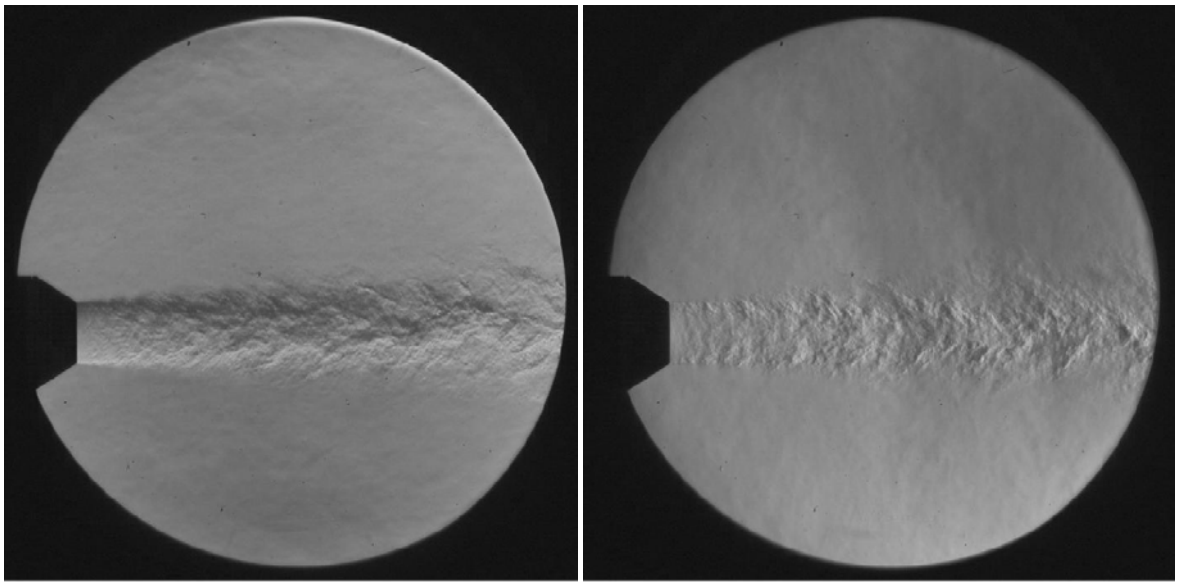

(a) **(b)**

Figure 15. Schlieren flow visualization of $L_e/D_e = 0.7$ at $PR_1 = 1.39$, $ER = 1.00$, $PR_2 = 1.39$, unheated configuration: (a) transverse density gradients, and (b) axial density gradients.

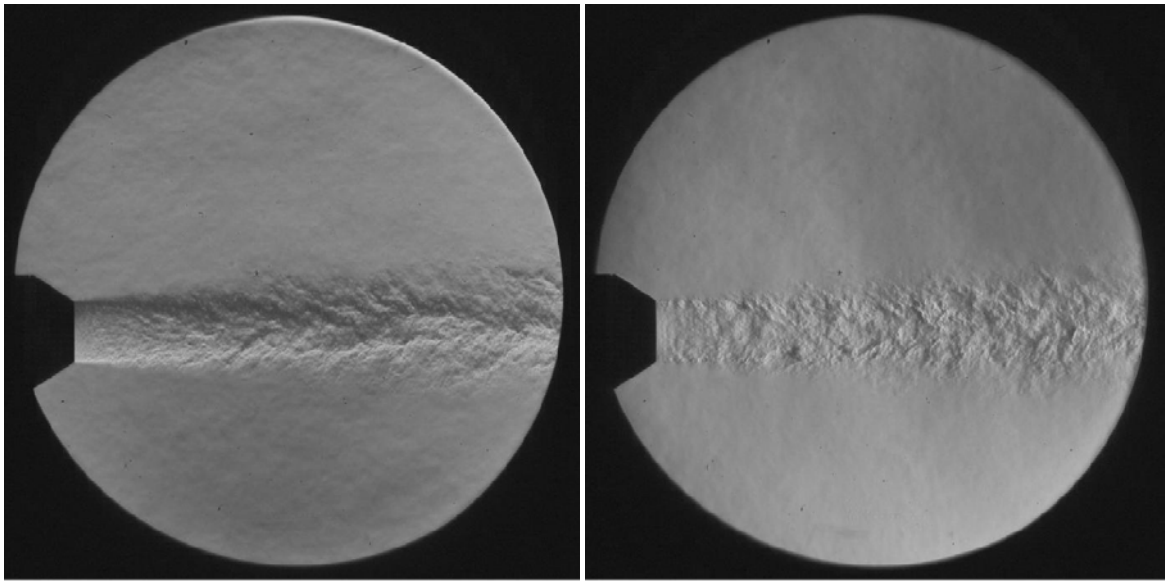

(a) **(b)**

Figure 16. Schlieren flow visualization of L_e/D_e = 0.7 at $PR_1 = 1.52$, $ER = 1.00$, $PR_2 = 1.52$ unheated configuration: (a) transverse density gradients, and (b) axial density gradients.

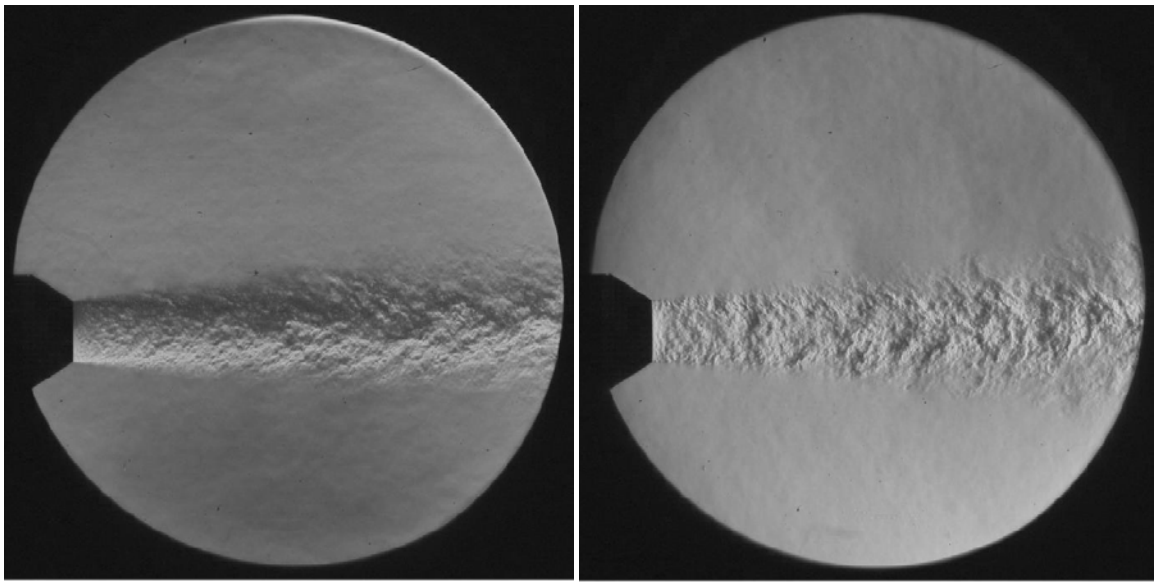

(a) **(b)**

Figure 17. Schlieren flow visualization of L_e/D_e = 0.7 at $PR_1 = 1.89, ER = 1.00, PR_2 = 1.89$, unheated configuration: (a) transverse density gradients, and (b) axial density gradients.

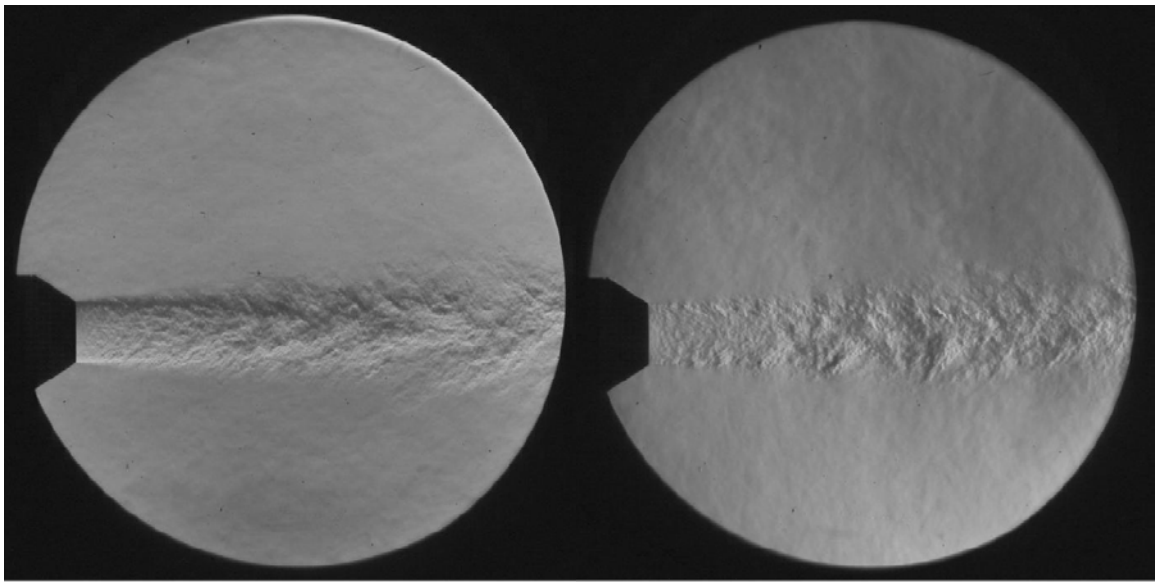

(a) **(b)**

Figure 18. Schlieren flow visualization of L_e/D_e = 0.7 at $PR_1 = 1.39$, $ER = 1.07$, $PR_2 = 1.49$, unheated configuration: (a) transverse density gradients, and (b) axial density gradients.

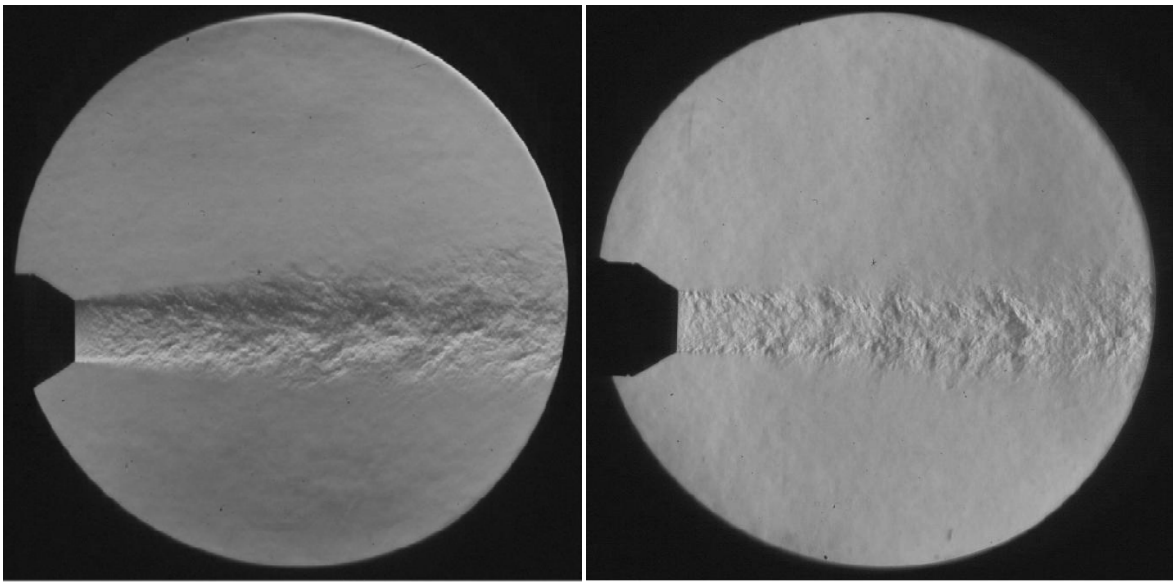

(a) **(b)**

Figure 19. Schlieren flow visualization of $L_e/D_e = 0.7$ at $PR_1 = 1.39$, ER = 1.10, PR_2=1.52 unheated configuration: (a) transverse density gradients, and (b) axial density gradients.

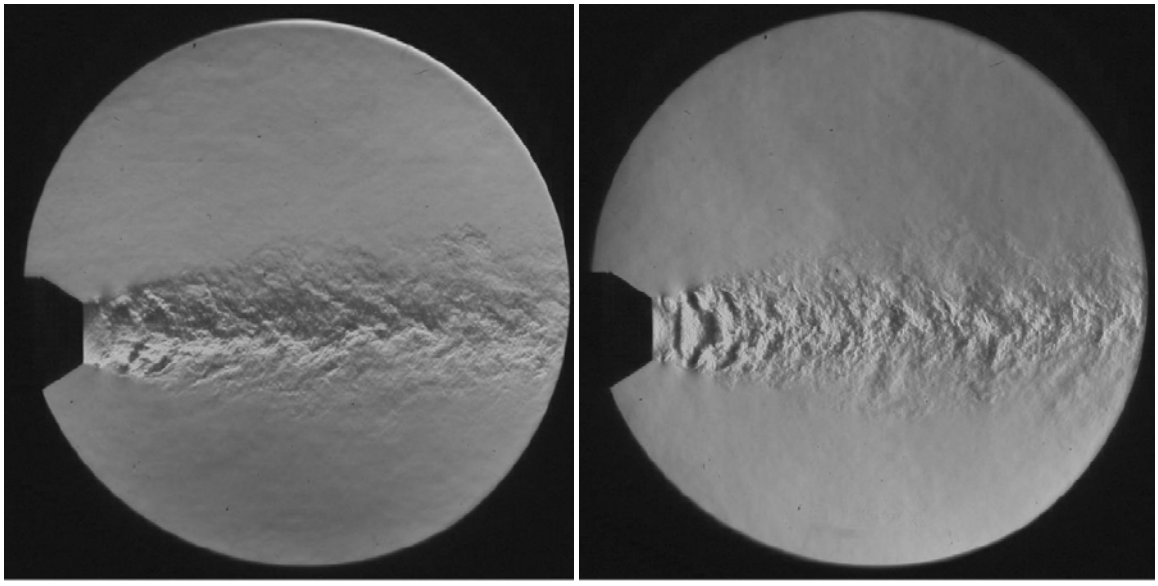

(a) **(b)**

Figure 20. Schlieren flow visualization of L_e/D_e=0.7 at $PR_1 = 1.69, ER = 1.00, PR_2 = 1.69$, unheated configuration: (a) transverse density gradients, and (b) axial density gradients.

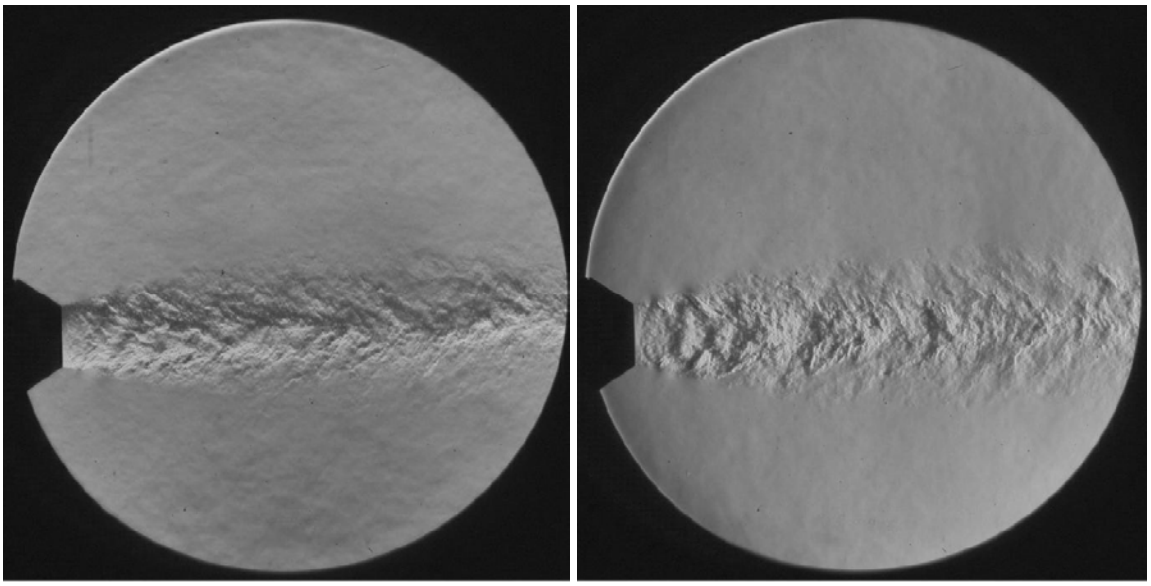

(a) **(b)**

Figure 21. Schlieren flow visualization of L_e/D_e=2.0 at $PR_1 = 1.69, ER = 1.00, PR_2 = 1.69$, unheated configuration: (a) transverse density gradients, and (b) axial density gradients.

Acoustic Measurements of Mechanical Tabs as a Forced Mixer

Facility Setup and Testing Description

The test model was mounted in the GTRI Anechoic Jet Facility for the acoustic data acquisition as seen in Figure 22. This facility is described in detail in Burrin et al. (1974), Burrin and Tanna (1979), and Ahuja (2003). Figure 23 shows the definitions of the polar (θ) and azimuthal (ϕ) angles used in positioning the microphones in the jet facility. Farfield microphones were mounted on polar arcs at angles between 30˚ and 120˚ with respect to the jet axis in 10˚ increments using the convention shown in Figure 23a. Three arcs were present during testing at azimuthal angles of 0˚, 45˚, and 90˚, as defined in Figure 23b. The jet upstream conditions were set by controlling the ratio of the total pressure to the ambient pressure (PR = p_t/p_a) for both the primary and secondary streams. Both the primary and secondary streams were varied between pressure ratios of 1.12 and 1.89. The extraction ratio (ER = p_{t2}/p_{t1}) was used as another parameter to define the secondary pressure ratio for a given primary stream pressure. Per insight and advice received from GAC and FAA, ERs between 1.00 and 1.07 are the most realistic conditions for a given PR_1 for mixed-flow conditions. In the unheated tests, the primary total temperature varied between 60˚F and 70˚F; and, during heated testing, it was set nominally to 500˚F. As a note, in this program the pressure ratio, PR, will refer to the ratio between upstream total and ambient pressures. In addition to the acoustic measurements, the primary and secondary total pressure and temperature, the primary and secondary mass flow rates (measured at the control valve), and the ambient pressure, temperature, and relative humidity were measured.

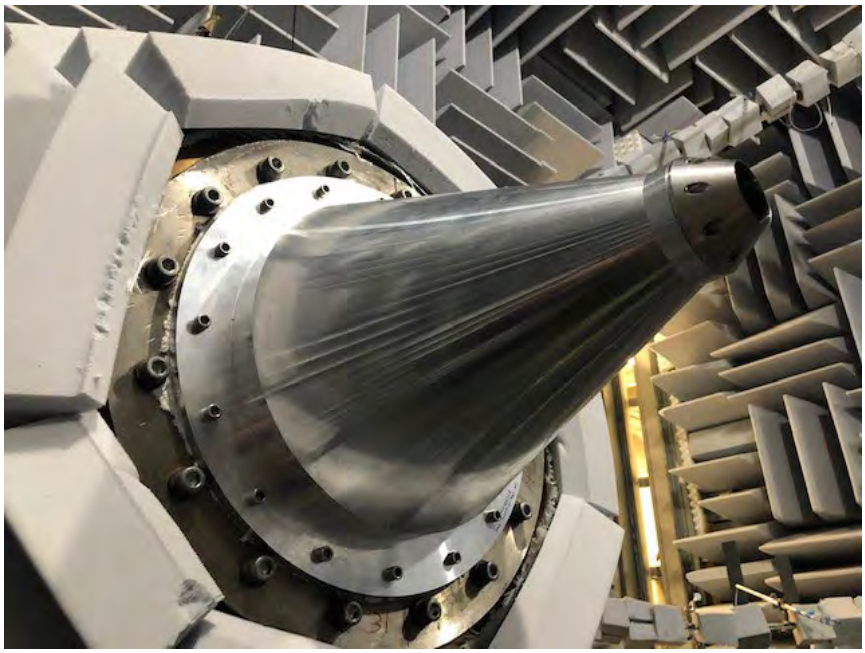

Figure 22. Project model set up in the Georgia Tech Research Institute Anechoic Jet Facility.

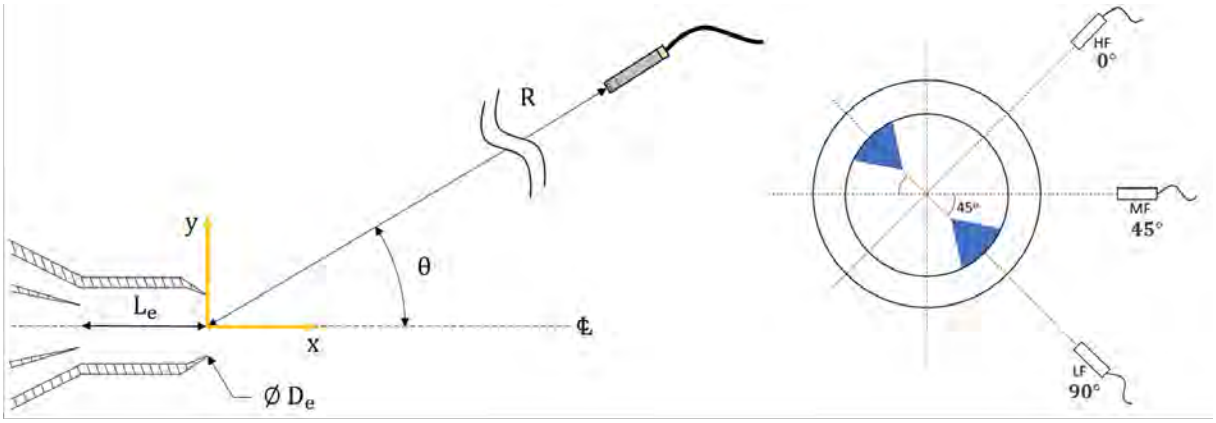

a) b)

Figure 23. Polar and azimuthal angle conventions.

The GTRI used two types of microphones that have the same performance. The first type are Bruel and Kjaer (B&K) 4939 ¼-in. free-field microphones and are attached to B&K 2669 preamplifiers. The B&K microphone-preamplifier combinations are connected to B&K 2960-A-0S4 Nexus conditioning amplifiers that, in addition to amplifying the signal, act as the microphones' 200 mV power supply. The second type of microphones are PCB Piezotronics Type 378C01 pre-polarized ¼-in. free-field microphones. These microphones utilize the IEPE capability so are powered directly from the data acquisition modules without a separate power supply. The microphone signals are sampled at 204.8 kHz using NI PXIe-4499 modules. The acoustic pressure time histories are then processed into averaged sound pressure level (SPL) spectra using a window size of 6,400 samples, 50% overlap, and a Hanning window. To render the data to lossless form for use by the modelers, the

following corrections are applied to these SPL spectra: free-field response correction, windsock correction (if necessary), atmospheric attenuation, and distance. These corrections are described in detail in Karon (2016).

Effect of the D-tabs on the Jet Noise Produced by the Confluent Nozzle

As stated above, the main focus of the Year 2 efforts is using mechanical tabs as a geometrically simple forced mixer. Mechanical, 3D-printed D-tabs were added to the interior of the core nozzle of the pre-existing confluent nozzle. Figure 24 shows this nozzle geometry, with the D-tabs installed at the core nozzle exit shown in red. In the context of a single nozzle, installing mechanical tabs near the nozzle exit plane that protrude into the jet flow is known to produce a substantial increase in mixing between the jet and the ambient relative to a tab-free nozzle (Ahuja, 1990). No prior published works have explored the use of mechanical tabs in lieu of more complex lobed mixers in an internally mixed nozzle. The findings of this research might shed light on the behavior of tabs as an alternative forced mixer geometry. Additionally, this was a good intermediate exercise while a forced mixer, described later, was being designed for the Year 3 effort.

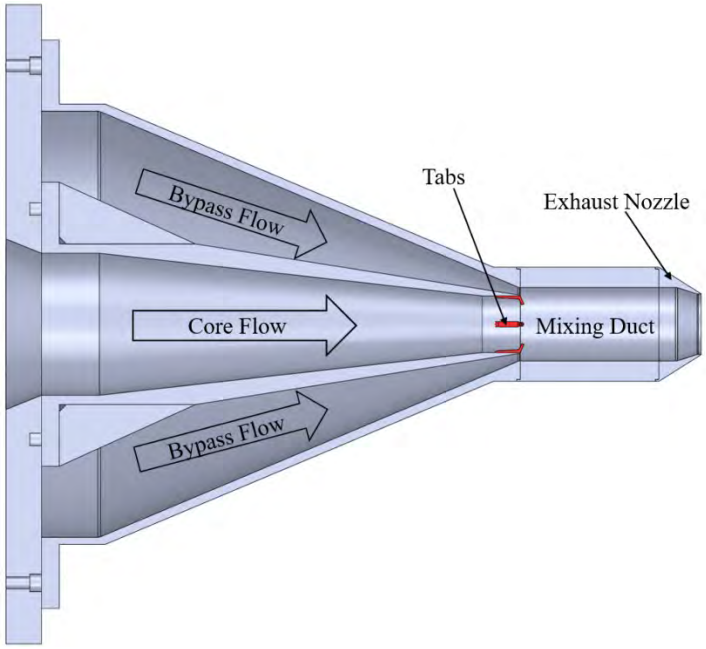

Figure 24. Cross-section of the nozzle configuration with the D-tabs installed. Tabs are shown in red.

Farfield jet noise measurement conducted with the confluent nozzle during year 1 revealed that, under certain operating conditions, the nozzle produced tonal noise (accompanied by radical changes to the resultant jet flow field). One hypothesis is that some of these tones are caused by a feedback mechanism inside the mixing duct. The first leg of this hypothetical feedback mechanism would involve the growth of a shear-layer instability (i.e., instability of the core-jet shear layer) inside the mixing duct and subsequent interaction of a large-scale coherent structure with the exhaust nozzle lip or other solid surfaces inside the nozzle. Farfield jet noise measurements acquired with the confluent nozzle equipped with tabs will shed light on the validity of this hypothesis. In short, adding tabs is likely to inhibit the growth rate of large-scale coherent structures before they may interact with the lip of the exhaust nozzle. Various configurations of the confluent nozzle equipped with tabs were tested, with the configurations shown in Figure 25. Although a wide range of conditions were tested, the following results are presented as typical results: PR_1 = 1.39 and ER = 1.0, PR_1 = 1.69 and ER = 1.0, and PR_1 = 1.39 and ER = 1.07. The tabs were tested with the confluent nozzle in both L_e/D_e = 0.7 and 3.0 configurations.

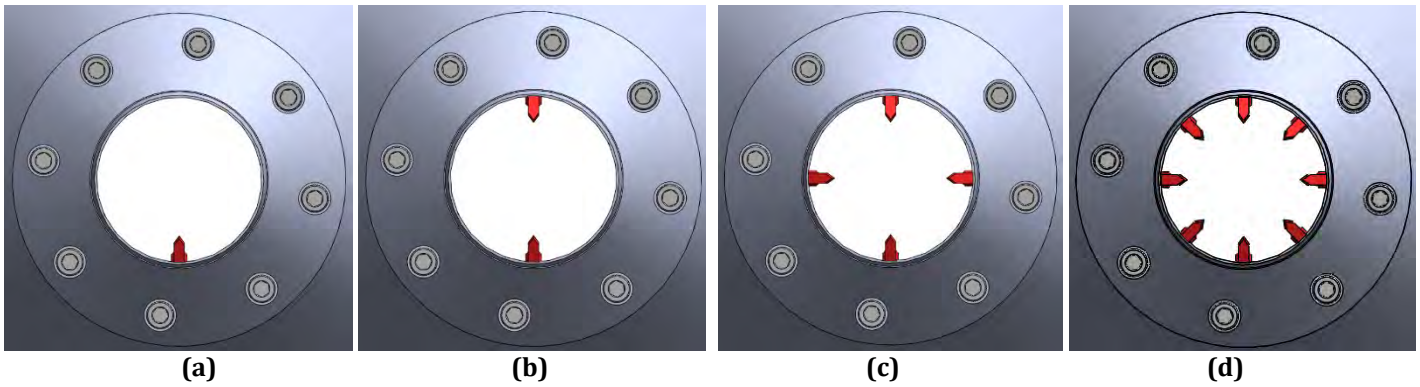

Figure 25. View looking upstream into tab-equipped internally mixed nozzle in (a) single-tab, (b) two-tab, (c) four-tab, and (d) eight-tab configurations.

Figures 26 and 27 show the effect on the jet noise produced by adding tabs to the core nozzle at the PR_1 = 1.39 and ER = 1.0, for mixing lengths L_e/D_e = 0.7 and 3.0, respectively. As shown in Figure 26, for L_e/D_e = 0.7, no tab configuration had any appreciable effect on the noise. Similarly, as shown in Figure 27, for L_e/D_e = 3.0, tabs, irrespective of the number used, had no appreciable effect at low frequencies (the left of the spectral peak), but increasing the tab number to four and then to eight seemed to increase the noise at higher frequencies. In particular, the noise at high frequencies is elevated by a maximum of 2 dB. These level increases begin at 20 kHz for the four-tab case and at 7 kHz for the eight-tab case.

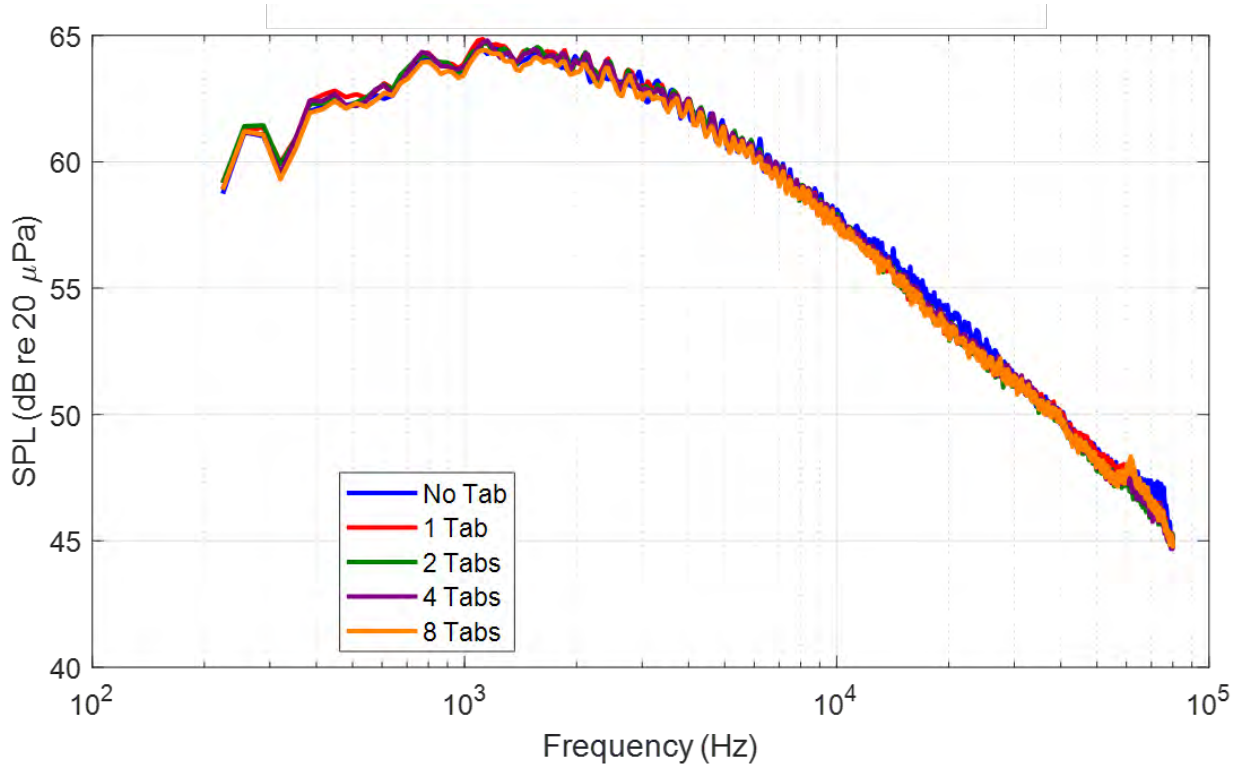

Figure 26. Effect of tabs on noise from a confluent nozzle. FAA Project Model, D_e = 1.7 in. and L_e/D_e = 0.7. PR_1 = 1.39, ER = 1.0, unheated, R = 12 ft, θ = 90°, Δf = 32 Hz, lossless.

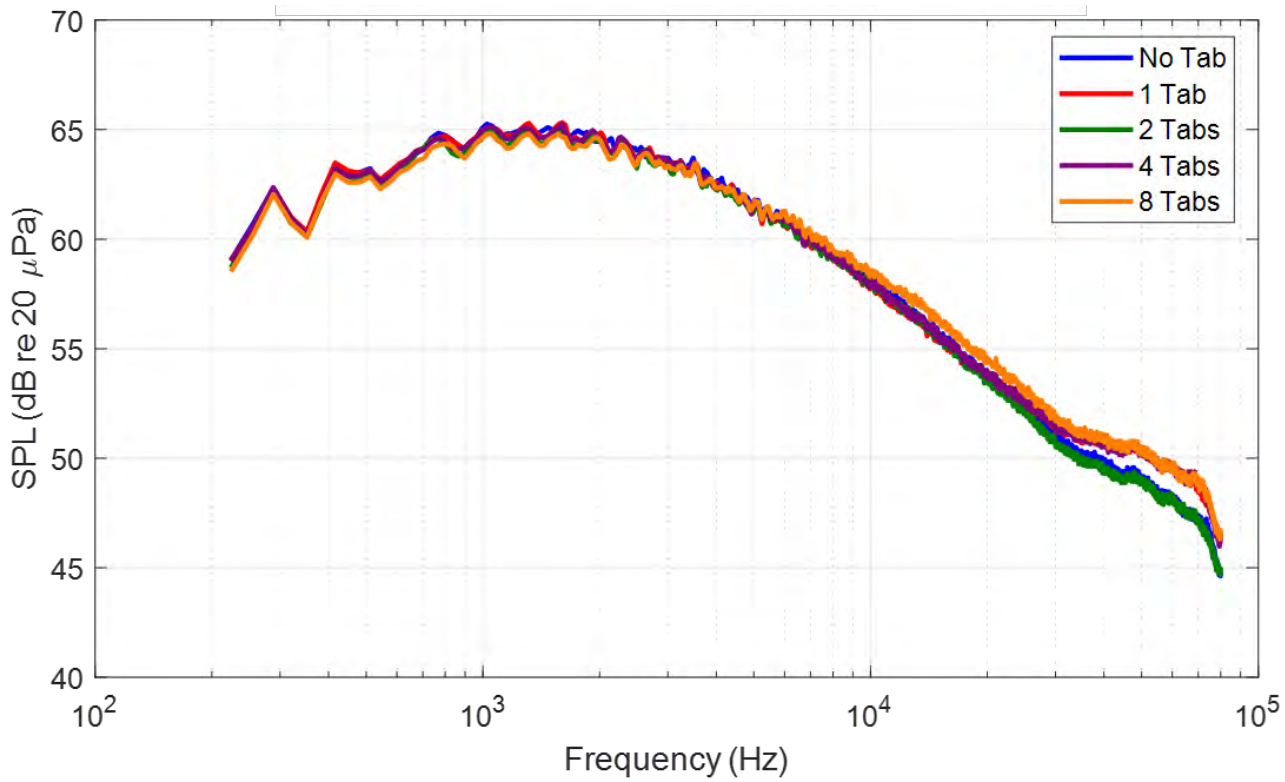

Figure 27. Effect of tabs on the noise from a confluent nozzle. FAA Project Model, D_e = 1.7 in. and L_e/D_e = 3.0. PR_1 = 1.39, ER = 1.0, unheated, R = 12 ft, θ = 90°, Δf = 32 Hz, lossless.

As has been previously presented, the confluent nozzle at the condition of PR_1 = 1.69 and ER = 1.0 produces tones that excite the jet flow. If the tone is the result of a feedback phenomenon, boundary layer perturbation via tabs is known to eliminate the tone. A well-known example is the case of suppressing screech by inserting the tip of a screw driver at the exit of a shock-containing jet. Figures 28 and 29 show the effect on the jet noise produced by adding tabs to the core nozzle at this condition, for mixing lengths L_e/D_e = 0.7 and 3.0, respectively. The tone is *not* eliminated by any of the tab configurations. Observing Figure 28, the addition of one or two tabs results in a maximum of 2 dB reduction in broadband noise over the frequency range of 1 kHz to 13 kHz, whereas the other tab configurations have no effect on the broadband noise. Looking at the effect on the tones alone, the one- and two-tab configurations cause the tone to shift to a higher frequency by 1.6 kHz and decrease in tonal amplitude by about 5 dB. The four- and eight-tab configurations cause a minor tone frequency shift of less than 200 Hz, with a 2–3 dB reduction in the tonal level.

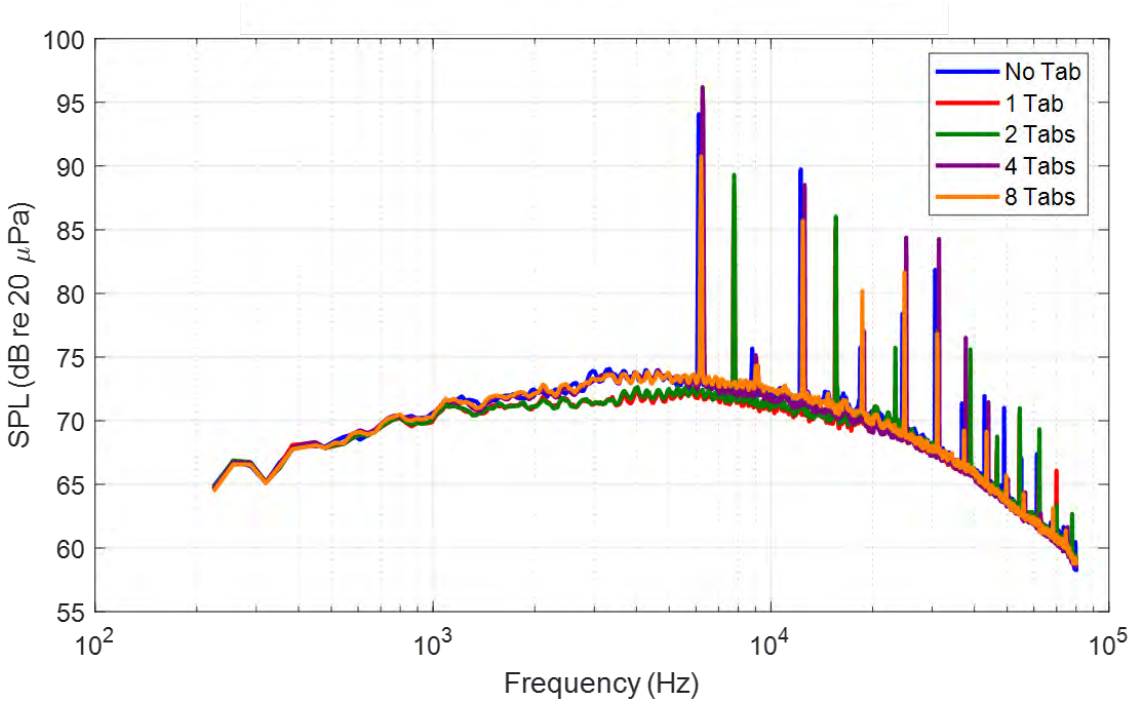

Figure 28. Effect of tabs on the noise from a confluent nozzle. FAA Project Model, D_e = 1.7 in. and L_e/D_e = 0.7. PR_1 = 1.69, ER = 1.0, unheated, R = 12 ft, θ = 90°, Δf = 32 Hz, lossless.

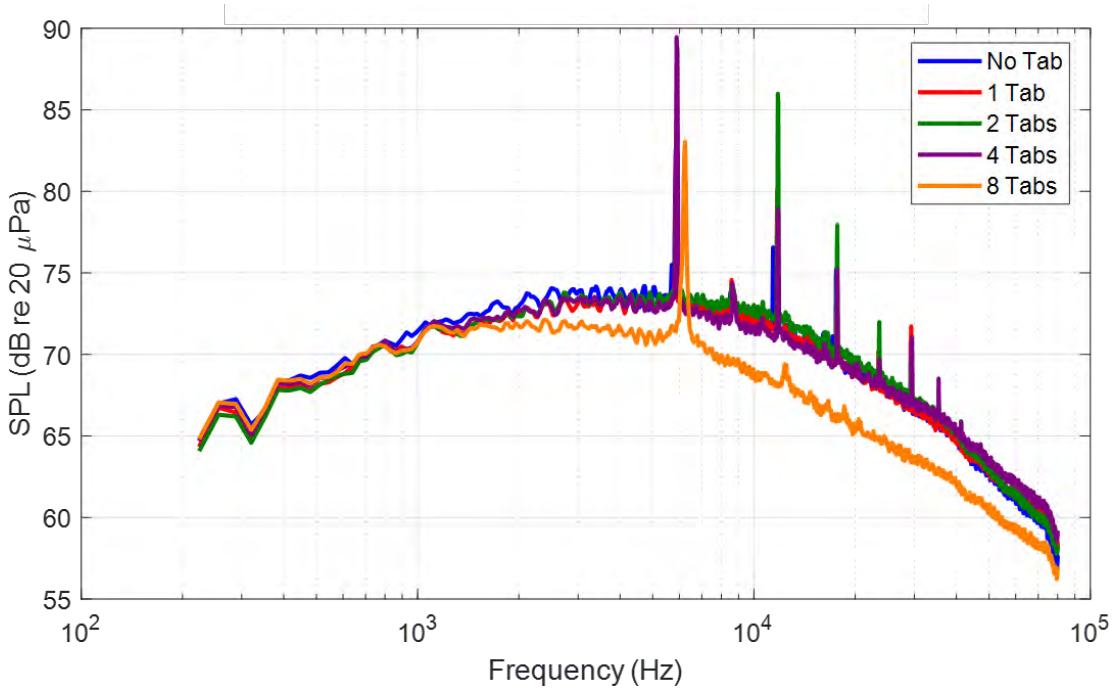

Figure 29. Effect of tabs on the noise from a confluent nozzle. FAA Project Model, D_e = 1.7 in. and L_e/D_e = 3.0. PR_1 = 1.69, ER = 1.0, unheated, R = 12 ft, θ = 90°, Δf = 32 Hz, lossless.

The effect of the tabs on L_e/D_e = 3.0 configuration differs significantly from that of the L_e/D_e = 0.7 configuration, as shown in Figure 29. It can be seen that all tab configurations except the eight-tab configuration produce essentially the same broadband noise as the no-tab configuration. The eight-tab configuration reduces the broadband noise by as much as 3 dB starting at frequencies above 2 kHz. Only one dominant tone is seen for this configuration, which has shifted to the right by about 400 Hz compared to that for the no-tab case and is also lower in amplitude. The other tab configurations produce the same tone frequency as the no-tab confirmation, but the levels of the harmonics increase with the number of tabs. No immediate explanations are available for this result.

The results shown in the last two figures were for an extraction ratio of unity. When the extraction ratio was increased to 1.07, the tones seen in the above figures mostly disappeared, as shown in Figures 30 and 31, which show the effect of the tabs on the noise produced by the confluent nozzle for PR_1 = 1.39 and ER = 1.07 for L_e/D_e = 0.7 and 3.0, respectively. For both mixing duct lengths, the tabs do not seem to make substantial difference. The exception to this is the one- and two-tab configurations, which generate a high-frequency tone for L_e/D_e = 0.7.

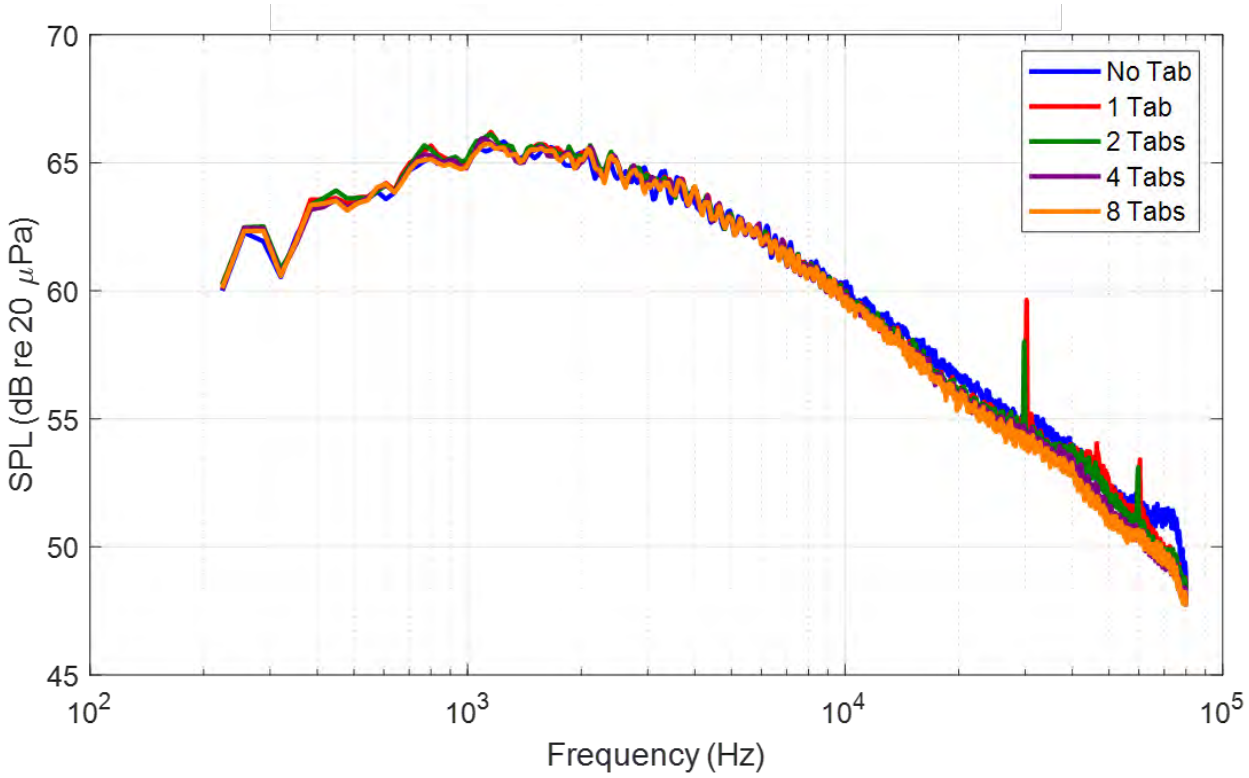

Figure 30. Effect of tabs on the noise from a confluent nozzle. FAA Project Model, D_e = 1.7 in. and L_e/D_e = 0.7. PR_1 = 1.39, ER = 1.07, unheated, R = 12 ft, θ = 90°, Δf = 32 Hz, lossless.

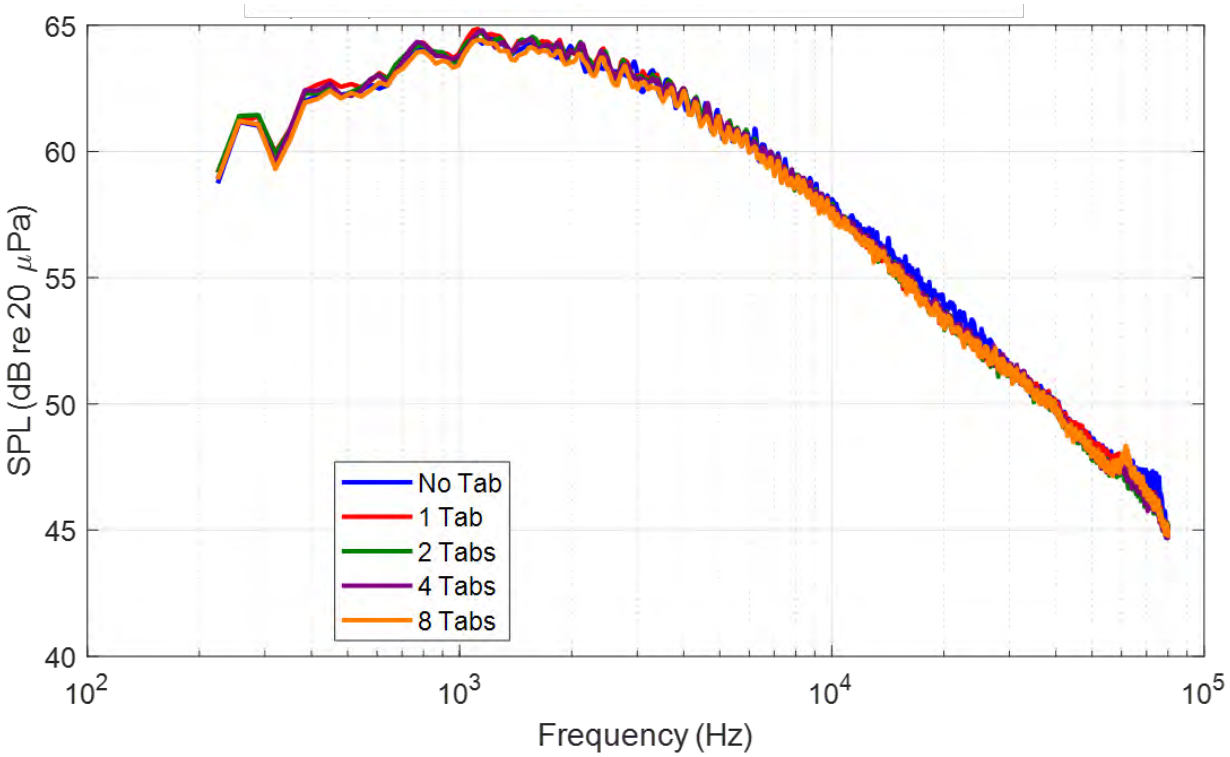

Figure 31. Effect of tabs on the noise from a confluent nozzle. FAA Project Model, D_e = 1.7 in. and L_e/D_e = 3.0. PR_1 = 1.39, ER = 1.07, unheated, R = 12 ft, θ = 90°, Δf = 32 Hz, lossless.

Effect of the Delta-Tabs on the Jet Noise Produced by the Confluent Nozzle

As described above, in addition to testing the D-tabs, delta-tabs (as shown in Figure 4) were tested for their effects on the noise produced by the confluent nozzle. For this set of testing, two tabs were installed as shown in Figure 5b. Figure 32 shows the effect of the azimuthal angle on the noise produced by the confluent nozzle with two metal delta-tabs attached to the core nozzle for the condition of PR_1 = 1.39, ER = 1.0 and at a polar angle of θ = 90°. The inset image in Figure 32 shows the orientation of the tabs with respect to the microphones for the readers' reference. As can be seen in Figure 32, at frequencies below 10 kHz, the noise without tabs and with tabs at all azimuthal angles is the same. Above 10 kHz, the tabbed nozzle case showed 3-dB increases at all azimuthal angles. At frequencies above 30 kHz, the ϕ = 90° direction seems to converge back with the no-tab case; the reason for this is not clear and would require additional analysis.

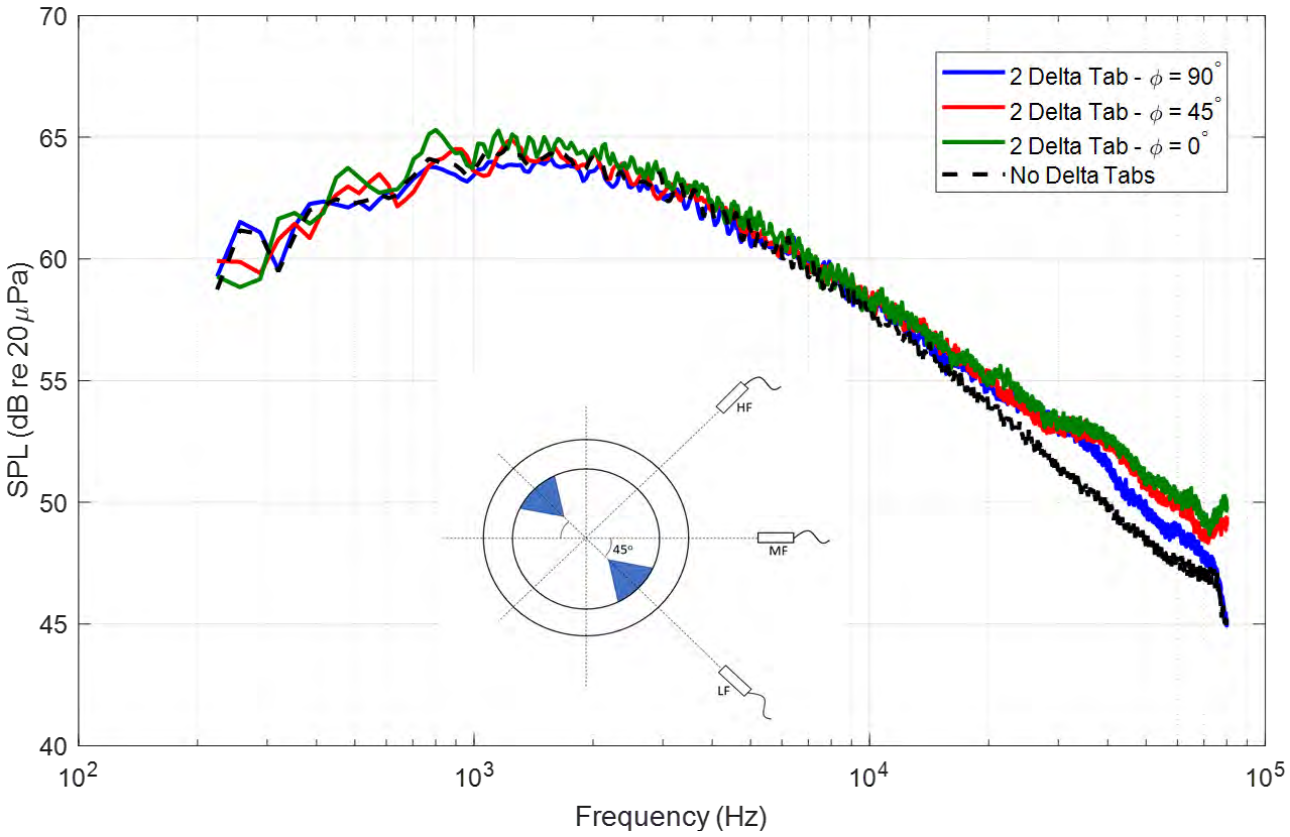

Figure 32. Effect of delta-tabs on the noise from the nozzle. D_e = 1.7 in, L_e/D_e = 0.7. PR_1 = 1.39, ER = 1.00, Tt,1 = Tt,2 = 60°F, R = 12 ft, θ = 90°, Δf = 32 Hz, lossless.

Figures 33 and 34 show the effect of the two delta-tabs on the jet noise spectra at PR_1 = 1.39, ER = 1.0, with a heated core flow ($T_{t,1} \approx 500$°F) at polar angles of 30° and 90°, respectively. As in Figure 32, Figures 33 and 34 show three azimuthal angles. In the rear-arc as shown in Figure 33, the delta-tabs create a 3-dB decrease in the peak noise at all azimuthal angles. Above 6 kHz, the delta-tabs actually increase the noise by as much as 4 dB. Additionally, at frequencies above 6 kHz, there is a difference in the azimuthal angles. Between 6 kHz and 35 kHz, the azimuthal angle aligned with tab produces up to 3 dB lower noise than the other azimuthal angles. Above, 35 kHz the azimuthal angles converge. In the sideline angle, as shown in Figure 34, at frequencies below 7 kHz, the tabs do not have any effect on the noise. Above 7 kHz, the tabs create an up to 3 dB increase in noise.

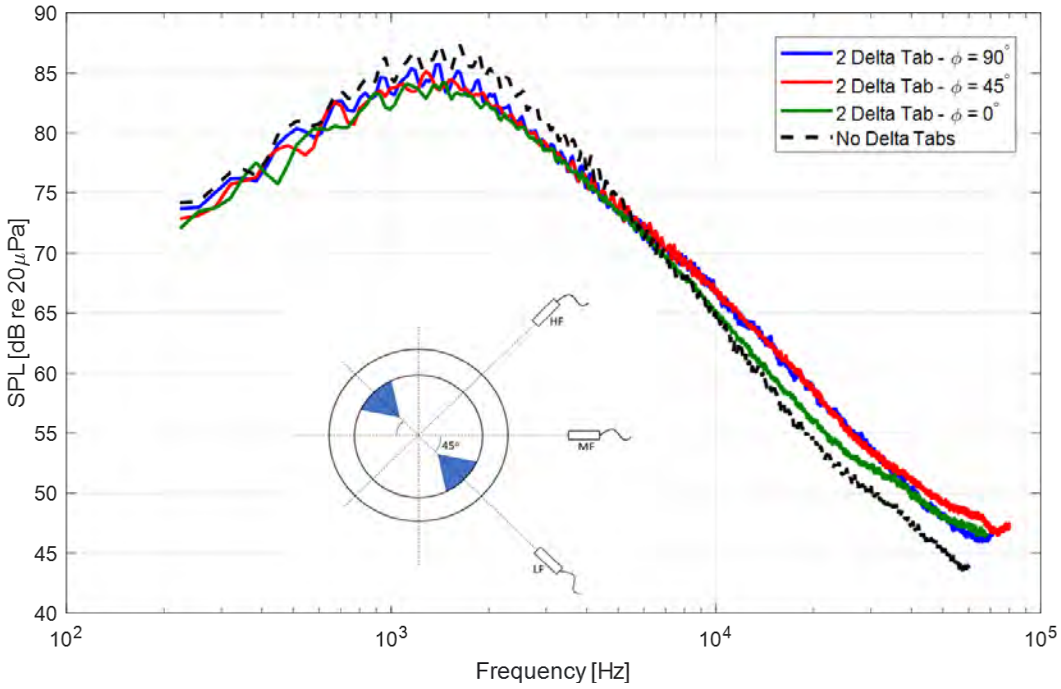

Figure 33. Effect of delta-tabs on the noise from the confluent nozzle. D_e = 1.7 in, L_e/D_e = 0.7. PR_1 = 1.39, ER = 1.00, Tt,1 = 500˚F, Tt,2 = 60˚F, R = 12 ft, θ = 30˚, Δf = 32 Hz, lossless.

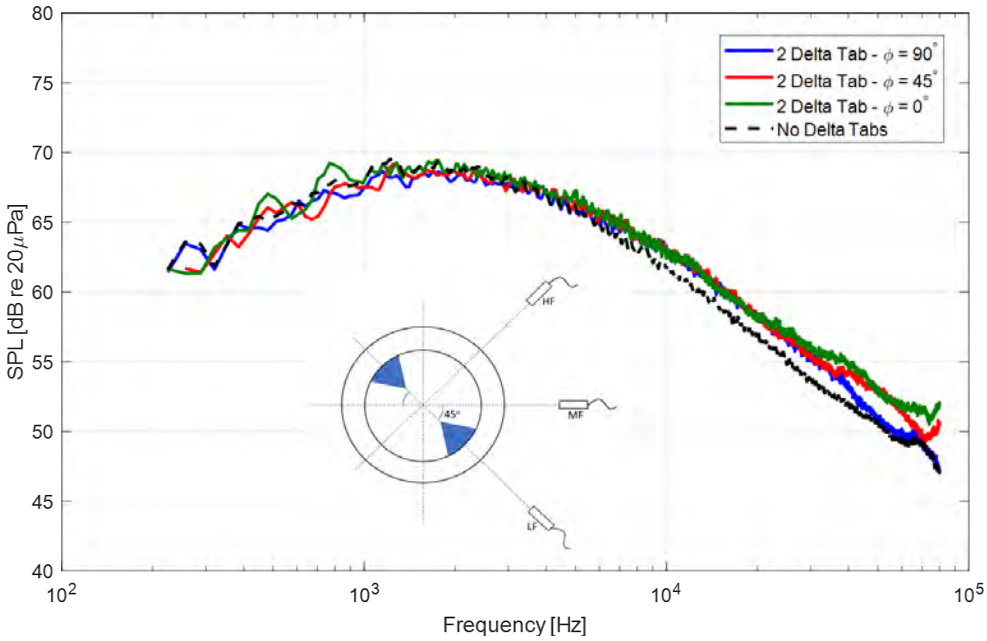

Figure 34. Effect of delta-tabs on the noise from the confluent nozzle. D_e =1.7 in, L_e/D_e = 0.7. PR_1 = 1.39, ER = 1.00, Tt,1 = 500˚F, Tt,2 = 60˚F, R = 12 ft, θ = 90˚, Δf = 32 Hz, lossless.

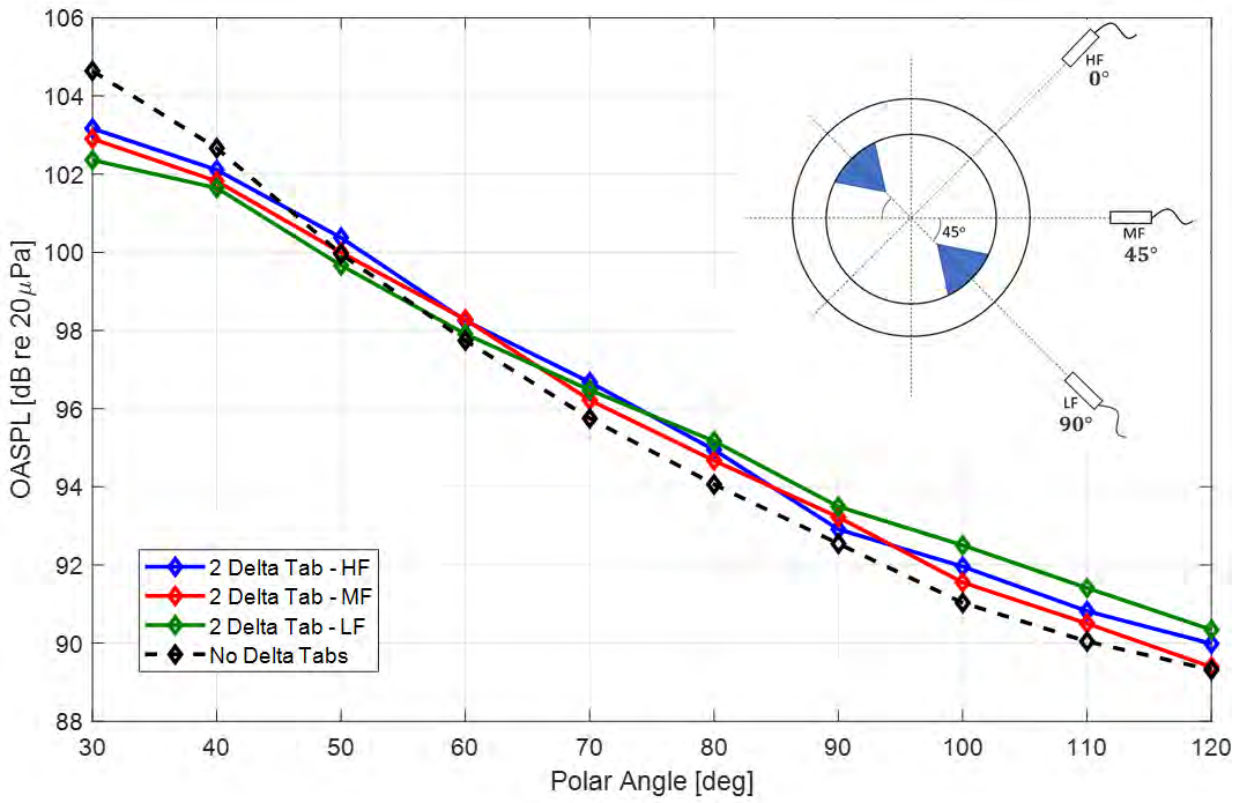

Figure 35. Effect of delta-tabs on the noise from the confluent nozzle. D_e = 1.7 in, L_e/D_e = 0.7. PR_1 = 1.39, ER = 1.00, Tt,1 = 500˚F, Tt,2 = 60˚F, R = 12 ft, Δf = 32 Hz, lossless.

At the same PR_1 = 1.39, ER = 1.00, $T_{t,1}$ = 500˚F operating condition, the effect of two delta-tabs on overall SPL (OASPL) is shown in Figure 35. At a polar angle of 30˚, where OASPL is greatest, a decrease of 1.5-2.3 dB is observed, depending on the azimuthal angle. In general, a decrease in OASPL exists at the lowest polar angles. At polar angles above 60˚, tabs always produce an increase in OASPL. Maximum OASPL increases of 0.5-1.4 dB (depending on azimuthal angle) occur at a 110˚ polar angle. Additionally, a trend of azimuthal dependency of OASPL is seen in Figure 35. When the observation angle is parallel to the line-of-symmetry of the delta-tabs, greater effects due to delta-tabs are seen relative to the other two measured azimuthal angles (both a greater OASPL reduction at smaller polar angles and greater OASPL increase at larger polar angles). Finally, the decrease in low-polar-angle OASPL and increase in high-polar-angle OASPL indicate that the delta-tabs yield enhanced interstream mixing compared to the tab-free confluent nozzle. These trends of low-polar-angle, low-frequency noise reduction at the cost of increased high-frequency noise been reportedly offered by lobed mixers as well (Mengle, 1997). The conclusion that the tabs have improved the interstream mixing between the core and bypass flows relative to the tab-free confluent nozzle is currently rooted purely in the acoustic measurements, and future work will include flow measurements of the jet plume produced by the confluent nozzle with tabs added to the core nozzle.

Similar results for chevrons were shown by Alkislar et al. (2007), where chevrons on a single nozzle enhanced mixing of jet exhaust flow and ambient air. This mixing broke up large-scale turbulent structures that propagate downstream toward low polar angles, and therefore increase small-scale turbulence that is dominant at higher polar angles. It is postulated that delta-tabs in the core nozzle are causing a similar behavior; however, flow visualization will be done to gain more information on the behavior of the jet with the implementation of the delta-tabs.

Comparison of D-Tabs and Delta-Tabs

Figures 36 and 37 show farfield jet-noise spectra acquired at polar angles of 30˚ and 90˚ (at an azimuthal angle of 45˚ from the tab, see Figure 23) with the nozzle run at the PR_1 = 1.39, ER = 1.00 operating condition. Each of these figures highlights the effects of adding either two 3-D printed delta-tabs or D-tabs to the core nozzle inside the confluent nozzle. As shown in Figure 36, the presence of either type of tab is shown to make no difference on the noise in the rear-arc. This shows that any noise produced by the tabs does not exceed contributions by the jet mixing noise. Alternatively, in the sideline, as shown in Figure 37, the D-tabs create noise reduction of up to 1 dB at the spectral peak and up to 2.5 dB at frequencies above 10 kHz, whereas the delta-tabs actually increase noise by up to 1.5 dB at frequencies above 10 kHz.

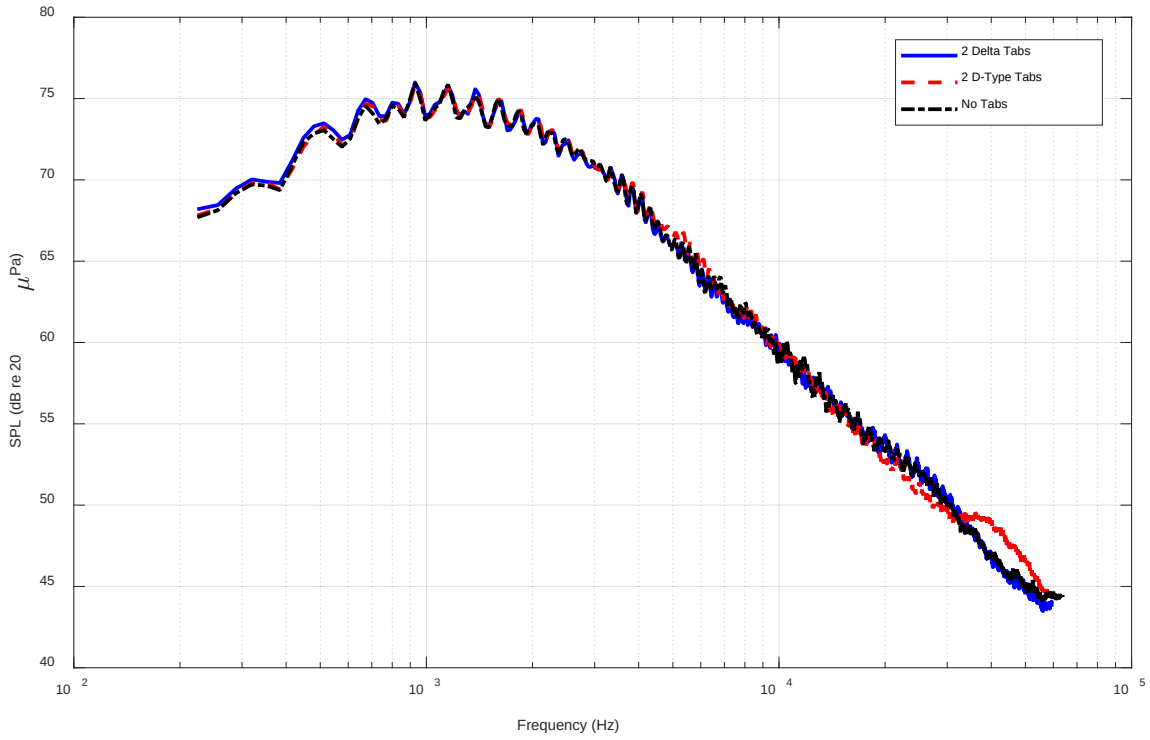

Figure 36. Jet noise generated by FAA nozzle with and without tabs in the core nozzle. D_e = 1.7 in, L_e/D_e = 0.7. PR_1 = 1.39, ER = 1.00, Tt,1 = Tt,2 = 60˚F, R = 12 ft, θ = 30˚, ϕ = 45˚, Δf = 32 Hz, lossless.

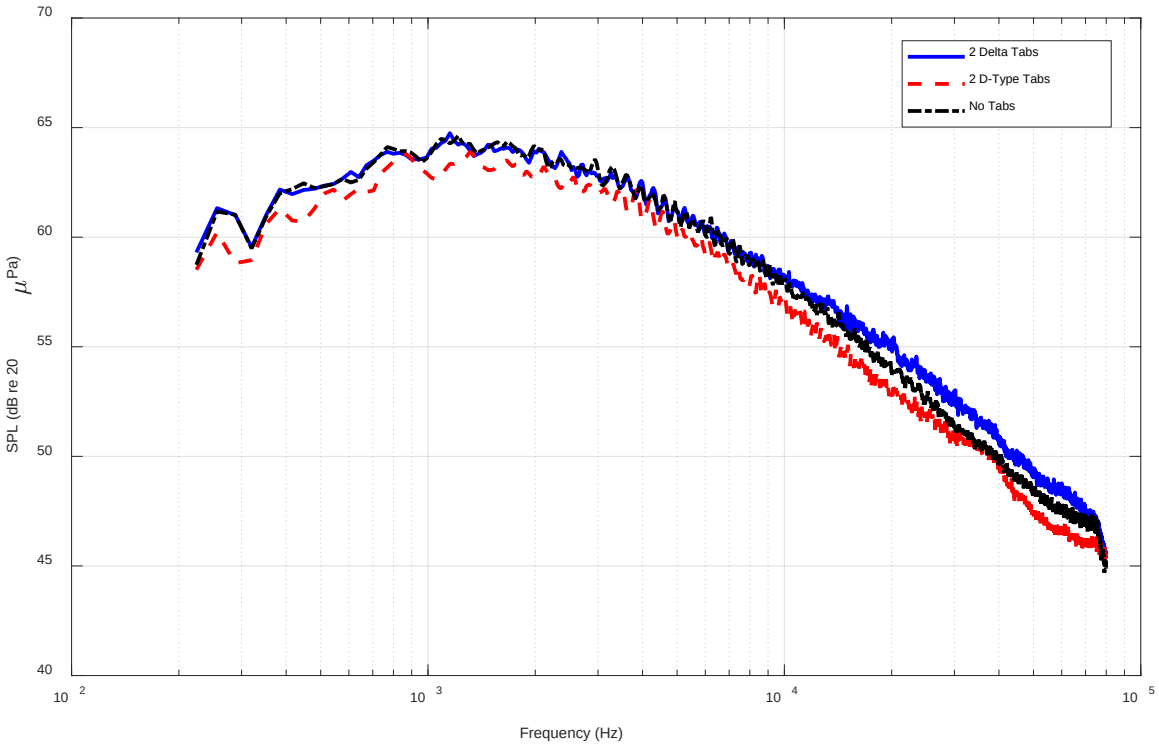

Figure 37. Jet noise generated by FAA nozzle with and without tabs in the core nozzle. D_e = 1.7 in, L_e/D_e = 0.7. PR_1 = 1.39, ER = 1.00, Tt,1 = Tt,2 = 60°F, R = 12 ft, θ = 90°, ϕ = 45°, Δf = 32 Hz, lossless.

Additional Understanding of Tones

Several publications discuss the importance of exhaust-nozzle design in the context of dual-stream, internally mixed nozzles. In particular, rapid changes in nozzle-wall angle (relative to the nozzle centerline) between the convergent and final straight sections of the final exhaust nozzle have been found to give rise to an additional noise source when forced mixers are used [19, 20]. This additional noise source was high frequency (relative to the frequency of peak jet noise), broadband in nature, directed toward θ = 70° with respect to the downstream jet axis, and appeared at high-subcritical pressure ratios. This noise source was attributed to the interaction between turbulence produced by the forced mixing of the two streams inside the nozzle and a shock near the exit plane of final exhaust nozzles with rapid changes in nozzle-wall angle. Final exhaust nozzles with more gradually contoured walls did not yield this additional noise source (Garrison, 2005). The shock near the final exhaust nozzle exit was found to terminate regions of supersonic flow that existed, despite the ideally expanded velocity of the flow being subsonic. This was hypothesized to be due to "flow turning effects" associated with the rapid change in nozzle-wall angle (Garrison, 2005). The region of supersonic flow was confined to a volume of fluid near the inner wall final exhaust nozzle, downstream of its return to straight. As noted by Garrison et al. (2005) and emphasized here, the associated additional noise source did not appear with a confluent nozzle (i.e., without a forced mixer) regardless of exhaust nozzle design. Nonetheless, the work of Garrison et al. is relevant here because they showed that final exhaust nozzles with rapid changes in nozzle-wall angle gave rise to an unfavorable flow phenomenon at high-subcritical pressure ratios.

The confluent nozzle used in the present work utilizes a final exhaust nozzle that has a rapid change in nozzle-wall angle before its final straight section – much like the nozzles studied by Garrison et al. (2005) that produced an unfavorable flow phenomenon. This, combined with the fact that the confluent nozzle produces a resonance at ER = 1.00, unheated operating conditions at high-subcritical pressure ratios (but not at lower pressure ratios), provides reason to believe that the exhaust nozzle's geometry may play a role in this resonance. This is not to say that the exhaust nozzle contains regions of supersonic flow at these operating conditions like those shown in the computational fluid dynamic predictions by Garrison et al. (2005);

however, it seems that the final exhaust nozzle is a likely region in which unfavorable flow phenomena may occur at high-subcritical pressure ratios.

To explore the hypothesis that the final exhaust nozzle geometry plays a role in setting up the resonance at PR_1 = 1.69 (M_j = 0.9), ER = 1.00, unheated operating conditions, several boundary-layer-tripping experiments were conducted, the most of which is described here. A trip ring was installed in the final exhaust nozzle's converging section as shown in Figure 38a and 38b. This trip ring was fashioned out of lock wire with a 0.5-mm diameter and was retained by four, roughly equally spaced rectangles of duct tape (approximately 0.45 mm thick). As shown by the sideline jet-noise spectra acquired with and without this trip ring in Figure 39, the addition of the trip ring suppresses the resonance entirely. The tones and the broadband amplification of jet noise associated with excitation of the jet both vanish, leaving behind a typical jet-noise spectrum (Ramsey, 2022). This is a powerful result. Regardless of the full, detailed physics underlying the confluent nozzle's resonance at this operating condition, the resonance is eliminated by a simple addition of a boundary-layer trip to the final exhaust nozzle geometry. The present resonance is therefore apparently driven by laminar boundary-layer separation (based on the success of a boundary-layer trip in suppressing it), and thus has striking similarity to the transonic resonance of the converging-diverging nozzles studied by Zaman and Dahl (1999). Yet more work is needed to obtain a rigorous understanding of the resonance in the present work. Nonetheless, some additional discussion is offered below.

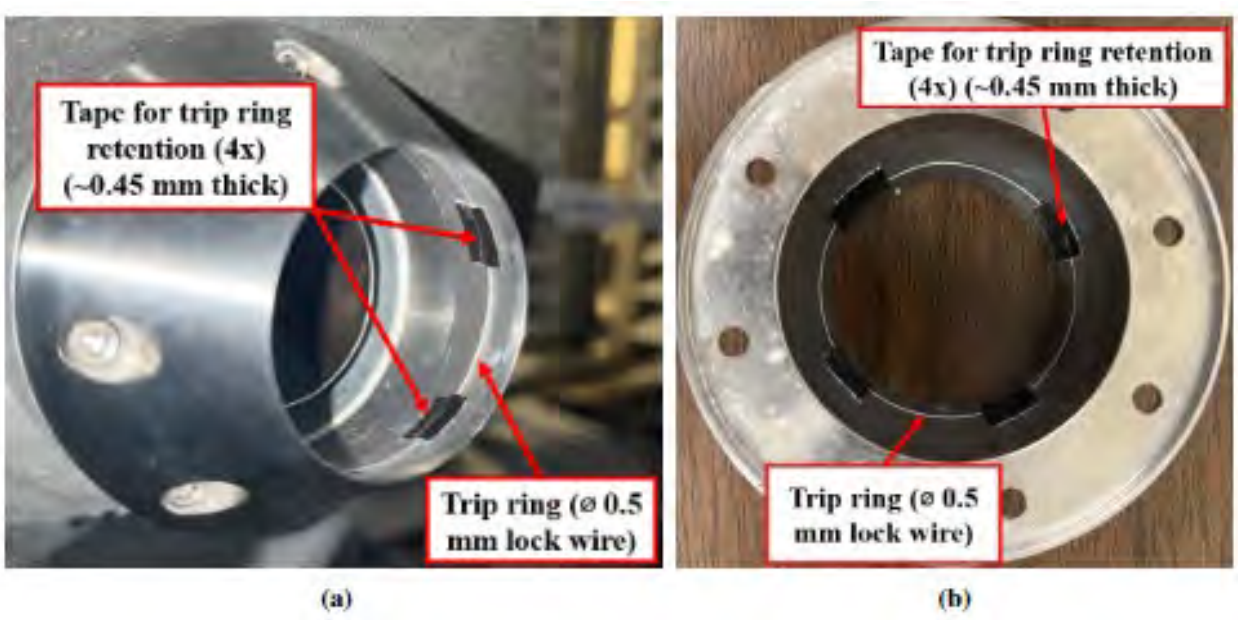

Figure 38. Boundary-layer trip configurations: (a) view from exit, and (b) view from upstream.

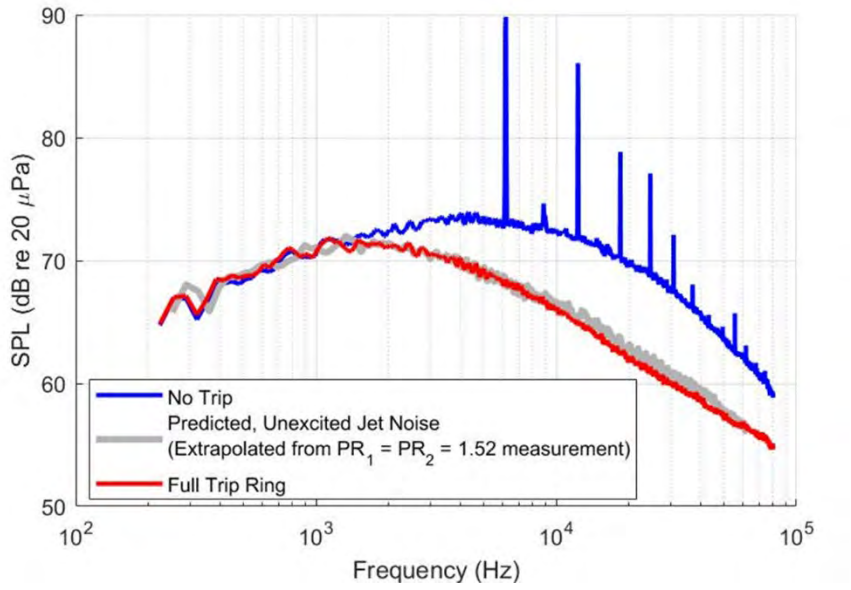

Figure 39. Effect of the boundary-layer trip ring on the noise from a confluent nozzle. FAA Project Model, D_e = 1.7 in. and L_e/D_e = 0.7. PR_1 = 1.69, ER = 1.0, unheated, R = 12 ft, θ = 90°, Δf = 32 Hz, lossless.

One possible explanation for the strength of the acoustic tones produced is that a resonant feedback loop is set up in the final straight section of the exhaust nozzle. As a hypothetical example, this feedback loop could comprise a downstream-travelling convective flow instability initiated at the exhaust nozzle's radius before the final straight section, sound generation due to this instability's interaction with the final exhaust nozzle lip, the upstream propagation of this sound, and the receptivity of the sound by a later flow instability. This is similar to the feedback considered in the study by Zaman and Dahl (1999). The existence of this feedback loop remains a hypothesis to be tested, and jet-noise measurements with fine increments in Mach-number between M_j = 0.9 and M_j = 1.0 at unheated, ER = 1.00 operating conditions with no boundary-layer trip are planned by Nate Ramsey for his PhD thesis funded by NSF. The results will be included in the FAA reporting as a value added to the program via his fundamental research. This will help elucidate the Mach-number dependence of this resonance and more clearly determine whether such a feedback loop is a plausible explanation. This focused testing is required because this ER = 1.00 resonance does not occur below $M_j \approx 0.9$ nor at M_j = 1.0, the two highest-pressure operating conditions tested as part of the larger test program. It is our hope that when the resonance is fully understood, the vanishing of the resonance at the sonic condition (M_j = 1.0) will become clear as well. This was not a feature of the resonances studied by Zaman and Dahl (1999).

It should be pointed out that because these results indicate that the tones may be a result of some feedback phenomenon associated with the flow just upstream of the final nozzle, anything done at the core nozzle may not have much impact on the tones. This indeed seems to be the case for the results shown above, where adding a smaller number of tabs did not have a major impact on tones. Where the tones were affected, that may be due to the flow arriving at the main nozzle exit being more turbulent with tabs than that without them. Additional work will be needed to understand the underlying phenomenon. It is felt that as long as we can eliminate the tones by a simple wire trip as described above, we will have high-quality data devoid of jet-noise amplification, simulating turbulent flows of a full-scale system and for validating the measurements.

Milestones

Conduct the following three sets of measurements for the baseline confluent nozzle configuration:

1. Flow visualization and PIV data for selected unheated flows for which extensive farfield acoustic data was acquired in Year 1.
2. Develop a methodology to eliminate the high-amplitude tones that were observed for certain operating test conditions in the Year 1 study.
3. Acquire acoustic data to quantify the effects of selected tab configurations on farfield jet noise.

Major Accomplishments
Met all of the above milestones.

Publications
None.

Outreach Efforts
None.

Awards
None.

Student Involvement
Three graduate students (David Nate Ramsey, Reagan Mayo, and Jackson Larisch).

Plans for Next Period
Complete heated flow data acquisition. Also, complete the design of a forced mixer.

Task 5 - Data Dissemination
Georgia Institute of Technology

Objective
The objective of this task is to maintain contact with the modelers being funded by FAA under ASCENT Project 59 and provide them with the nozzle design and both the acoustic and flow data from the current project.

Research Approach
This task involves disseminating the Year 2 data to the modelers. The modelers already have access to the data from the confluent nozzle as described in Task 0. We will release the geometries and available data from the nozzle equipped with tabs in the near future.

Milestones
Continue providing the modelers being funded by FAA under ASCENT Project 59 both the acoustic and flow data from the current project.

Major Accomplishments
All milestones met.

Publications
None.

Outreach Efforts
None.

Awards
None.

Student Involvement
Three graduate students (David Nate Ramsey, Reagan Mayo, and Jackson Larisch).

Plans for Next Period
None.

Task 6 - Design and Build a Mixer for Year 3 Investigation

Georgia Institute of Technology and Gulfstream Aerospace Corporation

Objective

The objective of this task is to design a sub-scale, realistic, internally mixed nozzle configuration with a lobed mixer for the primary nozzle.

Research Approach

A design capability has been developed for sizing, contouring, and surfacing of a forced multi-lobe mixer appropriate to medium bypass ratio turbofan engines. The process is initialized via analytic design of a confluent mixer and matching the static pressure on the mixing plane between the primary and secondary streams. The analytics can be optimized for ideal or thermally perfect (variable gamma) core flow. The confluent mixer performance is verified by CFD and confirmed to match performance characteristics in terms of bypass ratio, discharge coefficient, and velocity coefficient. Unsurprisingly, the confluent mixer offers limited thrust gain because mixing physics are limited to instability waves on the free shear layer between streams.

A lobed mixer is then designed to achieve target thrust gain characteristics for performance. The confluent mixer is treated as a neutral surface. Lobes are designed to flow hot core air into the space above the neutral surface. Gullies are designed to flow cool bypass air below the neutral surface. Scarfing and scalloping are used to enhance small-scale vortical structures on the mixing plane and realize mixing efficiencies two or three times greater than that for the confluent mixer design.

In a medium bypass ratio engine, this optimal mixing efficiency implies lobes and gullies with different penetration ratios. Design rules are developed to manage the asymmetry while still minimizing chute and mixing losses. Two-dimensional Bezier control curves are developed to meet the various design rules with three lofts specifying the (1) mixer trailing edge, (2) axial profile of the lobe, and (3) axial profile through the gully. These are intersected with the neutral surface to provide additional guide curves for construction.

A Python interface into Rhino3D is then used to loft the forced lobe mixer and complete surfacing. Geometry is exported to IGS and ready for either CFD or fabrication at a model shop. Initial design-of-experiments have been completed in RANS to check the design process and aero-thermodynamic performance. Initial proof-of-principle studies are complete, and we have initiated design of the actual mixer for the GTRI experiments.

A forced lobe mixer has been finalized for testing at GTRI. Static pressure matching at the mixing plane is achieved between streams, while ensuring good thrust gain due to mixing and protection of the nozzle inner mold line from unmixed core flow hot spot temperature distributions. A technical report is in development describing the design process and improvements that would logically lead to an optimal multidisciplinary solution.

The design has been checked for thermal distortions via a finite element analysis. Thickness distributions have been set slightly larger than implied by the geometric scale factor in order to ensure robustness and to ensure only modest deviations from the cold shape to hot shape. Actual estimates of hot shapes will be delivered to GTRI as part of the final geometry transmittal.

The 3D CAD geometry has been peer reviewed with GTRI, the FAA, and with ASCENT 59 university partners. An initial geometry has also been peer reviewed with the GAC model shop, and material has been ordered to ensure timely manufacturing. The parts will be released for manufacture as soon as an aero database has been completed and design performance has been verified across the range of intended operating conditions. Figure 40 depicts the lobed mixer.

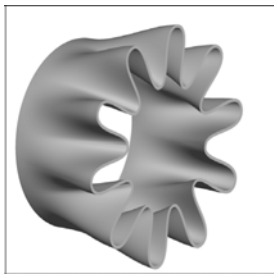

Figure 40. Depiction of the Gulfstream Aerospace Corporation (GAC)-designed lobed mixer.

Milestones
Complete the design of a sub-scale, realistic, internally mixed nozzle configuration with a lobed mixer for the primary nozzle.

Major Accomplishments
Two lobed mixers designed and will be available in Year 3 for testing.

Publications
None.

Outreach Efforts
None.

Awards
None.

Student Involvement
Three graduate students (David Nate Ramsey, Reagan Mayo, and Jackson Larisch).

Plans for Next Period
Fabricate the forced mixers for testing in Year 3. Also, acquire additional flow and acoustic data as needed to understand the observed flow/acoustic phenomenon.

Task 7 - Proposal for a Follow-on Effort for Year 3
Georgia Institute of Technology

Objective
The objective of this task is to prepare a proposal for a follow-on effort for Year 3.

Research Approach
This task involves preparing a proposal for Year 3 funding using a more complicated core nozzle. A forced lobe mixer configuration was selected. Georgia Tech's Cost-share partner Gulfstream will assist in designing and manufacturing the nozzle

Milestones
Submit a proposal to FAA to test a forced mixer that fits the existing test facility.

Major Accomplishments
The proposal was submitted in May 2022.

Publications
None.

Outreach Efforts
None.

Awards
None.

Student Involvement
Three graduate students (David Nate Ramsey, Reagan Mayo, and Jackson Larisch).

Plans for Next Period
If the project is funded, will begin testing the forced mixers.

Task 8 - Reporting and Data Dissemination
Georgia Institute of Technology

Objective
The objective of this task is reporting of the results acquired under Year 2 effort and disseminating the data to the modelers.

Research Approach
Submit all quarterly reports at the end of each quarter and the annual report at the end of the year. Prepare a quad chart for submission to the ASCENT Program as an update for the spring FAA ASCENT Advisory Committee meeting, and prepare a full progress presentation for the fall FAA ASCENT Advisory Committee meeting.

Milestones
- The experimental model was designed and fabricated.
- All acoustic measurements have been acquired.

Major Accomplishments
The experimental model was designed and fabricated. All acoustic measurements have been acquired.

Publications
Ramsey, D. N., Karon, A. Z., Funk, R., & Ahuja, K. K. (2022, June 14). Jet noise from a low-bypass confluent nozzle: Mixing length and extraction ratio effects. *28th AIAA/CEAS Aeroacoustics 2022 Conference*. 28th AIAA/CEAS Aeroacoustics 2022 Conference, Southampton, UK. https://doi.org/10.2514/6.2022-2863

Ramsey, D. N., Mayo, R., Karon, A. Z., Funk, R., & Ahuja, K. K. (2022, June 14). Self-excited jet from a low-bypass confluent nozzle at unity extraction ratio. *28th AIAA/CEAS Aeroacoustics 2022 Conference*. 28th AIAA/CEAS Aeroacoustics 2022 Conference, Southampton, UK. https://doi.org/10.2514/6.2022-2864

Outreach Efforts
None.

Awards
None.

Student Involvement
Three graduate students (David Nate Ramsey, Reagan Mayo, and Jackson Larisch).

Plans for Next Period

- Complete flow measurements
- Completed tab study
- Prepare for Year 3 efforts

References

Ahuja, K., & Brown, W. (1989, March 13). Shear flow control by mechanical tabs. *2nd Shear Flow Conference*. 2nd Shear Flow Conference, Tempe,AZ,U.S.A. https://doi.org/10.2514/6.1989-994

Hileman, J., & Samimy, M. (2003). Effects of vortex generating tabs on noise sources in an ideally expanded Mach 1.3 jet. *International Journal of Aeroacoustics*, *2*(1), 35–63. https://doi.org/10.1260/147547203322436935

Saiyed, N., & Bridges, J. (1999, May 10). Tabs and mixers for reducing low bypass ratio jet noise. *5th AIAA/CEAS Aeroacoustics Conference and Exhibit*. 5th AIAA/CEAS Aeroacoustics Conference and Exhibit, Bellevue, WA, U.S.A. https://doi.org/10.2514/6.1999-1986

Tam, C. K. W., & Zaman, K. B. M. Q. (2000). Subsonic jet noise from nonaxisymmetric and tabbed nozzles. *AIAA Journal*, *38*(4), 592–599. https://doi.org/10.2514/2.1029

Burrin, R. H., & Tanna, H. K. (1979). The Lockheed-Georgia coannular jet research facility. *The Journal of the Acoustical Society of America*, *65*(S1), S44–S44. https://doi.org/10.1121/1.2017259

Raffel, M., Willert, C. E., Scarano, F., Kähler, C. J., Wereley, S. T., & Kompenhans, J. (2018). *Particle image velocimetry: A practical guide*. Springer International Publishing. https://doi.org/10.1007/978-3-319-68852-7

Bridges, J. & Wernet, M. P. (2011). The NASA subsonic jet particle image velocimetry (PIV) dataset (NASA TM-2011-216807). https://ntrs.nasa.gov/api/citations/20110023688/downloads/20110023688.pdf

Pope, S. B. (2000). *Turbulent flows* (1st ed.). Cambridge University Press. https://doi.org/10.1017/CBO9780511840531

Christensen, K. T. (2004). The influence of peak-locking errors on turbulence statistics computed from PIV ensembles. *Experiments in Fluids*, *36*(3), 484–497. https://doi.org/10.1007/s00348-003-0754-2

Ahuja, K., Lepicovsky, J., Tam, C., Morris, P, & Burrin, R. (1982). *Tone-Excited Jet: Theory and Experiments* (NASA CR-3538). https://ntrs.nasa.gov/api/citations/19830004698/downloads/19830004698.pdf

Witze, P. O. (1974). Centerline velocity decay of compressible free jets. *AIAA Journal*, *12*(4), 417–418. https://doi.org/10.2514/3.49262

Morris, P. J., & Zaman, K. B. M. Q. (2010). Velocity measurements in jets with application to noise source modeling. *Journal of Sound and Vibration*, *329*(4), 394–414. https://doi.org/10.1016/j.jsv.2009.09.024

Burrin, R. H., Dean, P. D., & Tanna, H. K. (1974). A new anechoic facility for supersonic hot jet noise research at lockheed - georgia. *The Journal of the Acoustical Society of America*, *55*(2), 400–400. https://doi.org/10.1121/1.3437223

Ahuja, K. K. (2003). Designing clean jet-noise facilities and making accurate jet-noise measurements. *International Journal of Aeroacoustics*, *2*(3), 371–412. https://doi.org/10.1260/147547203322986188

Karon, A. (2016). *Potential factors responsible for discrepancies in jet noise measurements of different* studies [Ph.D. Dissertation, Daniel Guggenheim School of Aerospace Engineering, Georgia Institute of Technology].

Ahuja, K. (1990, October 22). An evaluation of various concepts of reducing supersonic jet noise. *13th Aeroacoustics Conference*. 13th Aeroacoustics Conference, Tallahassee, FL, U.S.A. https://doi.org/10.2514/6.1990-3982

Mengle, V., Dalton, W., Bridges, J., Boyd, K., Mengle, V., Dalton, W., Bridges, J., & Boyd, K. (1997, May 12). Noise reduction with lobed mixers—Nozzle-length and free-jet speed effects. 3rd AIAA/CEAS Aeroacoustics Conference. 3rd AIAA/CEAS Aeroacoustics Conference, Atlanta, GA, U.S.A. https://doi.org/10.2514/6.1997-1682

Alkislar, M. B., Krothapalli, A., & Butler, G. W. (2007). The effect of streamwise vortices on the aeroacoustics of a Mach 0.9 jet. Journal of Fluid Mechanics, 578, 139–169. https://doi.org/10.1017/S0022112007005022

Garrison, L., Lyrintzis, A., Blaisdell, G., & Dalton, W. (2005, May 23). Computational fluid dynamics analysis of jets with internal forced mixers. *11th AIAA/CEAS Aeroacoustics Conference*. 11th AIAA/CEAS Aeroacoustics Conference, Monterey, California. https://doi.org/10.2514/6.2005-2887

Tester, B., & Fisher, M. (2006, May 8). A contribution to the understanding and prediction of jet noise generation by forced mixers: Part III Applications. 12th AIAA/CEAS Aeroacoustics Conference (27th AIAA Aeroacoustics Conference). Cambridge, Massachusetts. https://doi.org/10.2514/6.2006-2542

Ramsey, D. N., Mayo, R., Karon, A. Z., Funk, R., & Ahuja, K. K. (2022, June 14). Self-excited jet from a low-bypass confluent nozzle at unity extraction ratio. 28th AIAA/CEAS Aeroacoustics 2022 Conference. 28th AIAA/CEAS Aeroacoustics 2022 Conference, Southampton, UK. https://doi.org/10.2514/6.2022-2864

Zaman, K., & Dahl, M. (1999, January 11). Aeroacoustic resonance with convergent-divergent nozzles. 37th Aerospace Sciences Meeting and Exhibit. 37th Aerospace Sciences Meeting and Exhibit, Reno, NV, U.S.A. https://doi.org/10.2514/6.1999-164